Applied Energy 332 (2023) 120556

Contents lists available at ScienceDirect

Applied Energy

journal homepage: www.elsevier.com/locate/apenergy

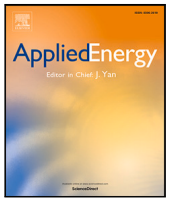

Experimental validation of a hybrid 1-D multi-node model of a hot water thermal energy storage tank

Iván De la Cruz-Loredo [a,*], Daniel Zinsmeister [b], Thomas Lickleder [b], Carlos E. Ugalde-Loo [a], Daniel A. Morales [a], Héctor Bastida [a], Vedran S. Perić [b], Arslan Saleem [a]

[a] Cardiff School of Engineering, Cardiff University, Queen's Buildings, The Parade, Cardiff, CF24 3AA, Wales, UK
[b] Munich Institute of Integrated Materials, Energy and Process Engineering (MEP), Technical University of Munich, Lichtenbergstraße, Munich, 85748, Germany

ARTICLE INFO

Keywords:
Thermal energy storage
Hot water tanks
Heating systems
Energy systems
Dynamic systems modelling

ABSTRACT

Hot water-based thermal energy storage (TES) tanks are extensively used in heating applications to provide operational flexibility. Simple yet effective one-dimensional (1-D) tank models are desirable to simulate and design efficient energy management systems. However, the standard multi-node modelling approach struggles to reproduce the dynamics of highly thermally stratified tanks due to their artificial numerical diffusion. In this paper, a novel 1-D multi-node modelling approach is introduced for accurately simulating water tanks with a high extent of thermal stratification. A non-linear, hybrid continuous–discrete time model able to capture the sudden temperature change within the tank is presented. The modelling approach was adopted to simulate a commercial TES tank, with the model being implemented in MATLAB/Simulink. Results from experimental tests were compared with simulation results, demonstrating that a hybrid continuous–discrete 12-node model accurately estimates the temperatures of the tank. It is also shown that the hybrid model avoids the numerical diffusion exhibited by standard multi-node models. This has been evidenced by the reduced root mean square and mean absolute errors exhibited by the hybrid model when compared with the experimental data.

1. Introduction

Thermal energy storage (TES) plants are widely used in thermal networks to allow their flexible operation through the efficient and timely management of thermal energy supply and demand [1]. This brings well-known environmental and economic benefits, such as the reduction of CO_2 emissions, lower energy generation costs, and reduced systems' operational costs [2]. Although different TES technologies with a higher energy density are available in the market such as those based on latent heat (and phase change materials), hot water TES units are extensively used due to their low cost, simplicity, and favourable thermal properties [3].

The analysis, dynamic simulation, and control design of hot water tanks may be facilitated by adopting one-dimensional (1-D) models which accurately predict their performance and state-of-charge (SoC). Simultaneously, these models must achieve a trade-off between accuracy and complexity to reduce their computational cost. The standard multi-node modelling approach is commonly adopted in the literature and available in commercial software due to its simplicity. Highly spatially discretised multi-node tank models are usually adopted to overcome the numerical diffusion inherent to the modelling approach for forced convection heat transfer and accurately capture sudden temperature transitions [4,5]. However, a high number of nodes increases model complexity and simulation times without guaranteeing the accuracy of the results.

An insightful comparison of 1-D multi-node tank models with a different number of nodes is carried out in [6] for two experimental hot water tanks. Although a direct relationship between the number of nodes and the accuracy of the model could be drawn during a charging process which exhibits significant flow disturbances at the inlet, the accuracy of the results observed in the discharging of the second tank is low. In addition, a reduced accuracy is observed when the number of nodes used to model the second tank increases. This decreased accuracy is especially noticeable for reduced water flow rates, which facilitate thermal stratification by preventing mixing within the tank [7]. Thus, 1-D models that accurately represent hot water tanks exhibiting a high extent of thermal stratification are still needed.

Although the verification of a few 1-D hot water tank models has been reported in the literature, the potential variations in the stratification and sudden temperature changes during charging and discharging operations have been mostly disregarded. Ref. [8] illustrates how significant these differences may be following a theoretical

* Corresponding author.
E-mail address: DeLaCruzLoredoI@cardiff.ac.uk (I. De la Cruz-Loredo).

https://doi.org/10.1016/j.apenergy.2022.120556
Received 19 August 2022; Received in revised form 22 November 2022; Accepted 18 December 2022
Available online 28 December 2022

Nomenclature

Subscripts

cin	Cold inlet node
$cin+1$	Node immediately above the cold inlet node
exp	Experiment measurement
hin	Hot inlet node
$hin-1$	Node immediately below the hot inlet node
i	Node i
$i+1$	Node $i+1$
$i-1$	Node $i-1$
$i \rightarrow i+1$	From node i to node $i+1$
$i-1 \rightarrow i$	From node $i-1$ to node i
$i \leftrightarrow i+1$	Between nodes i and $i+1$
$i \leftrightarrow i-1$	Between nodes i and $i-1$
j	Node j
$j+1$	Node $j+1$
$j-1$	Node $j-1$
k	Current discrete moment
$k+1$	Next discrete moment
l	Layer l
max	Maximum operating value
min	Minimum operating value
sim	Simulation measurement
st	Storage tank

Symbols

A_c	Cross-sectional area of the tank [m^2]
A_w	Area of the tank wall [m^2]
c_p	Specific heat coefficient [J/(kg °C)]
D_t	Diameter of the tank [m]
D_{in}	Diameter of the tank inlet [m]
g	Acceleration of gravity [m/s^2]
$\dot{H}$	Rate of change of the sensible heat [W]
k_f	Thermal conductivity coefficient of water between nodes [W/(m °C)]
k_m	Adjusting thermal conductivity coefficient between nodes [W/(m °C)]
MAE	Mean absolute error
N	Number of nodes in a multi-node tank model
n	Number of samples
$\dot{Q}_{FC}$	Forced convection heat transfer flow [W]
$\dot{Q}_{NC}$	Natural convection heat transfer flow [W]
$\dot{Q}_K$	Conductivity heat transfer flow [W]
$\dot{Q}_L$	Heat loss [W]
$\dot{Q}_G$	Heat flow from heat sources [W]
Ri	Richardson's number
RMSE	Root mean square error
SoC	State-of-charge [%]
SoC_m	Modified state-of-charge [%]
T	Temperature [°C]
T_a	Ambient temperature [°C]
T_c	Cold inlet temperature [°C]
T_h	Hot inlet temperature [°C]
T_{in}	Inlet temperature [°C]
$\mathbf{u}$	Input vector
U	Convective heat transfer coefficient between storage tank and environment [W/(m^2 °C)]
U_{FC}	Heat transfer coefficient between the storage tank and environment due to forced convection [W/(m^2 °C)]
U_0	Heat transfer coefficient between the storage tank and environment in standby condition [W/(m^2 °C)]
u_{in}	Linear velocity of the fluid at the tank's inlet [m/s]
V	Volume [m^3]
$\dot{V}_{in}$	Volumetric flow rate in the storage tank [m^3/s]
v_{th}	Linear velocity of the thermocline barrier [m/s]
$\mathbf{x}_c$	Continuous states vector
$\mathbf{x}_d$	Discrete states vector
y	Vertical position within the storage tank [m]
$\mathbf{y}$	Output vector
y_{th}	Vertical position of the thermocline [m]
z_a	Experimental measurement
$\hat{z}_a$	Model measurement
β	Coefficient of thermal expansion [$°C^{-1}$]
Δx	Height of a node [m]
Δt	Discrete time step [s]
ρ	Density [kg/m^3]

and experimental characterisation of thermal stratification for practical tanks. Therefore, accurate models with a reduced spatial resolution and easily adaptable for different thermal stratification conditions during charging and discharging are yet to be developed. Such less computationally intensive models would be desirable for a real-time accurate calculation of the tank's SoC, which would, in turn, lead to a more effective operation of a hot water tank within a heating system.

This paper presents a novel 1-D multi-node model based on hybrid continuous–discrete time systems. The modelling approach aims to increase the accuracy of standard 1-D multi-node models for simulating hot water tanks operating with a high extent of thermal stratification. The model includes a discrete variable to define the vertical position of a flat thermocline barrier used to describe where sudden temperature transitions occur within the tank. This is in turn used to update the reference temperature employed in the calculation of the node temperatures. The model is capable of:

1. Capturing the delayed temperature transition in the nodes due to the transport effect of the thermocline through the tank's height.
2. Reducing the numerical diffusion of the tank model without increasing its spatial resolution.
3. Accurately representing the extent of thermal stratification during charging and discharging of the tank by including the effect of the thermocline displacement in the calculation of node temperatures, as convenient.

A 1-D hybrid continuous–discrete time TES tank model with 12 nodes was implemented in MATLAB/Simulink, given the software's capabilities to simulate hybrid systems, and validated using experimental data of a complete charging and discharging cycle of an actual hot water TES unit. The hot water tank operates with a low thermal stratification during charging and a high thermal stratification during discharging. Thus, the variable capturing the effect of the thermocline

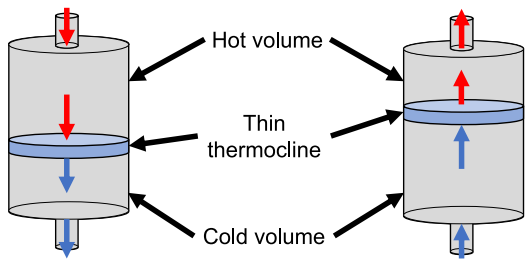

Fig. 1. Charging (left) and discharging (right) processes of a fully stratified TES tank.

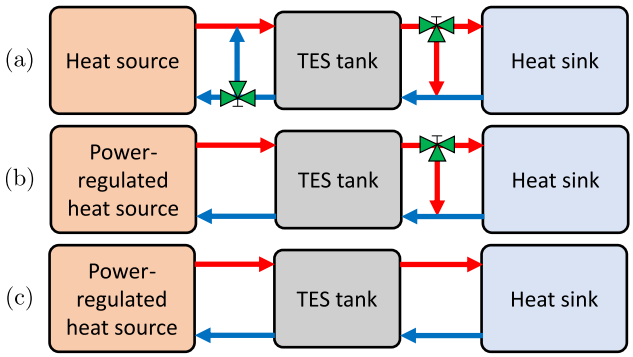

Fig. 2. System configurations for a hot water TES tank connected to: (a) a temperature-regulated heat source and a temperature-regulated heat sink; (b) a power-regulated heat source and a temperature-regulated heat sink; (c) a power-regulated heat source and an unregulated heat sink.

displacement was introduced during the discharging of the tank model only. For completeness, the simulation results obtained from the presented hybrid 12-node tank model were compared with those obtained using standard multi-node tank models. As demonstrated by an error analysis, the results from the hybrid 12-node tank model exhibit a good agreement with experimental temperature measurements and the SoC, enhancing the accuracy of the solution during the discharging process with respect to the standard tank models. It is also demonstrated that a standard 60-node model exhibits a reduced fidelity for calculating the temperature gradient and the SoC of the tank during the discharging process, regardless of its higher spatial resolution.

The remainder of the paper is organised as follows. Section 2 provides a background and literature review on the thermal stratification, characterisation, and 1-D multi-node modelling of hot water-based TES tanks. Section 3 introduces the 1-D hybrid continuous–discrete multi-node tank modelling approach. Section 4 describes the experimental setup and the model of the practical hot water TES tank investigated in the paper. Section 5 presents the experimental validation of the hybrid model and a comparison with the standard modelling approach. Section 6 discusses the limitations of the hybrid modelling approach. Finally, Section 7 presents the conclusions and brings the paper to a close.

2. Background and literature review

2.1. Thermal stratification of water-based TES tanks

The performance of water TES tanks depends on several factors, such as the effectiveness of the tank's insulation and the height of its inlet and outlet ports [9]. One of the most relevant aspects to consider is the thermal stratification of water (i.e. the temperature gradient) since highly thermally stratified tanks are more efficient than lowly stratified or unstratified tanks as they collect and supply heat at larger temperature differentials [10,11]. The temperature gradient between the hotter and colder zones within a TES tank is known as thermocline, and it is often used as a reference to evaluate the extent of thermal stratification [10].

Thermal stratification of practical TES tanks is established between two ideal conditions: a fully stratified tank and a fully mixed tank [10]. The fully stratified tank considers a thin thermocline dividing the tank's volume into two well-defined water volumes with different temperatures, namely hot and cold volumes. As shown in Fig. 1, the thermocline moves upwards or downwards in plug flow for charging or discharging the tank without mixing occurring between the water volumes. Thus, a sudden temperature change occurs through the tank's height as the thermocline moves. (**Note**: in a plug flow all particles in a cross-sectional area exhibit identical velocity and direction of motion [12].)

Different factors contribute to the mixture of volumes of hot and cold water within a storage tank, thus deteriorating its thermal stratification. Some references have investigated through experimental tests the effects that the location of the inlet port and its geometry, mass flow rate, aspect ratio of the tank, and the temperature difference between the inflow and the fluid inside the tank may have on thermal stratification. A key finding is that thermal stratification is enhanced by increasing the aspect ratio and inflow temperature differences [13,14]. However, the effect of the mass flow rate depends on the inflow temperature and the design of the inlet system [14,15]. A constant inlet temperature is recommended to maintain a high degree of thermal stratification [15].

An effective design of the inlet system combined with a strict control of the mass flow rate and inlet temperature may maximise the thermal stratification in a TES tank by reducing the mixing produced at the inlet [15,16]. However, achieving this is not trivial as inlet flow rates and temperatures depend on the configuration and control of the thermal source and the thermal sink connected to the tank. A poor design and control of heating systems may lead to high return temperature levels [17], which may impact the operation of a tank. For further information, the interested reader is referred to [18,19], where different control strategies for the integration of TES tanks into heating systems are discussed.

The extent of thermal stratification in a water tank may vary for charging and discharging operations. For example, Fig. 2 shows three different system configurations for a hot water tank connected to a heat source and a heat sink. In Fig. 2(a), the tank is connected to a temperature-regulated heat source and a temperature-regulated heat sink, where a by-pass valve is used to vary a mixture of hot and cold water flows to maintain a constant inlet temperature during charging and discharging. In this case, the system could be operated under a high thermal stratification condition (see Fig. 1). On the other hand, Fig. 2(b) shows a tank connected to a power-regulated heat source and a temperature-regulated heat sink. Mixing generated in the inlet port during charging cannot be avoided due to temperature variability and, therefore, the ideal high thermal stratification condition cannot be guaranteed during charging. Fig. 2(c) shows a tank connected to a power-regulated heat source and an unregulated heat sink. Mixing occurs at the inlet during both charging and discharging.

2.2. Richardson's number

Dimensionless numbers are often used to characterise thermal stratification in water tanks and evaluate their charging and discharging efficiencies (e.g. MIX number, tank aspect ratio, Reynolds number, Peclet number, and stratification number). A review and comparison of these numbers and an assessment of their sensitivity to relevant operating conditions of a tank can be found in [20,21]. Among the options, the Richardson's number is widely used to quantify the inlet mixing phenomena [14]. It describes the ratio of buoyancy forces on a flow that is at a different density than that of an immobile fluid (i.e. a quiescent fluid).

The Richardson's number considers the flow temperature and flow conditions in the inlet of the tank, the tank's geometry, and the type of inlets. Thus, its mathematical expression varies according to the design of the tank and inlets. An overview of mathematical descriptions used in the literature can be found in [21]. For a standard TES tank with side inlets and horizontal inlet flow, the Richardson's number Ri is given as

$$\mathrm{Ri} = \frac{g\beta D_t(T_{in} - T_{st})}{u_{in}^2} \tag{1}$$

where g [m/s^2] is the acceleration of gravity, β [1/°C] is the coefficient of thermal expansion of water, D_t [m] is the diameter of the tank, u_{in} [m/s] is the linear velocity of water at the inlet of the tank and T_{in} [°C] its temperature, and T_{st} [°C] is the temperature of the water within the tank.

Experiments reported in the literature have found that for Ri < 0.25 a significant inlet turbulence is generated, producing a significant mixing and contributing to the deterioration of the thermal stratification [21]. Conversely, high values of Ri indicate a large extent of thermal stratification in the water tank. Although values of Ri amenable to the formation of thin thermoclines have not been explicitly reported in the literature, maximum values are on the order of 100 [22].

2.3. Modelling of hot water tanks

References found in the literature have shown that 1-D models may retain a good degree of accuracy for temperature prediction in a TES tank whilst reducing the complexity of the model [23]. In contrast, three-dimensional (3-D) models can describe the internal thermal behaviour of the TES unit very accurately using finite element analysis (FEA) and computational fluid dynamics (CFD). For instance, ANSYS Fluent is an often-employed commercial software for 3-D modelling [24,25]. However, much simpler 1-D models are still desirable to simulate and study interactions of hot water tanks with other elements of heating systems and design control systems. For example, 1-D TES tank models have been employed to study the economic feasibility of residential combined heat and power units in [26]. 1-D tank models have also been used to design control systems for hot water tanks [27] and to design and investigate new demand-side control strategies for improving the operation of heating systems [19,28]. The design and implementation of real-time SoC estimation of TES tanks also require simple 1-D models for the data acquisition and control [29,30].

Commercial software engines for the simulation of dynamic processes can facilitate the modelling and simulation of hot water tanks since they nominally provide pre-defined standard models that can be quickly customised and simulated [31]. For example, a comparison of different prosumer configurations in district heating systems is carried out in [32] using 1-D tank models available in the software platform SimulationX. Further details on some popular commercial software engines for 1-D modelling and simulation of water TES tanks are provided in Appendix A.

1-D representations of thermally stratified water TES tanks use a finite volume discretisation approach to the total tank's volume [33,34]. A non-linear ordinary differential equation models the mass, momentum and energy balance in each discrete water volume or node. The number of nodes, also called the spatial resolution, is commonly associated with the fidelity of the thermal model [25,31]. Alternative models have been developed from the standard finite volume discretised model, aiming to capture different hydraulic phenomena occurring within the tank. For example, a 50-node TES tank model capturing the buoyancy and mixing effects in the inflow and outflow inlets is presented in [35]. Similarly, a 60-node model capturing the effect of a moving thermocline using an adaptive-grid approach is presented in [4], achieving similar temperature transitions to those from a standard multi-node model with a high spatial resolution. A Lagrangian modelling approach consisting of a tank with a varying number of segments (from 1 to up to 3000 segments) was compared against the standard multi-node tank model with fixed number of segments in [36], with similar simulation results.

2.4. Numerical diffusion in 1-D multi-node models

The main drawback of the 1-D multi-node modelling approach for hot water tanks is the artificial numerical diffusion involved in the temperature calculation of the nodes. This is generated by the spatial discretisation of the tank's volume when forced convection heat transfer occurs [4,37].

The tank's nodes are considered fully mixed water volumes with uniformly distributed temperatures. The forced water flow in the tank produces a heat transfer between the nodes, which modifies their temperatures. The rate of change of temperature in a node is calculated from the temperature of the adjacent nodes and the volumetric water flow rate. Since the heat transfer is considered to occur in the node's borders, nodes with large volumes exhibit a slower temperature transition (i.e. high numerical diffusion) than nodes with small volumes. Therefore, multi-node models with a high spatial resolution (i.e. high number of nodes) are often adopted to define nodes with smaller volumes and simulate fast temperature transitions in the tanks [4].

Although numerical diffusion may be reduced in models with nodes of small volumes, this cannot be totally avoided. By having a larger number of nodes, an increased number of equations must be solved, also increasing the computational cost. Besides, models with high spatial resolution may also lead to significant simulation errors, as shown in Section 5 of this paper. Due to the calculation method, the rate of change of temperature in nodes is progressive throughout the tank from the node where water is directly injected (inlet) to the node where water is subtracted (outlet). Since the nodes' temperatures are modified for the slightest temperature difference between adjacent nodes, a faster response in the nodes close to the tank's inlet also produces a faster response for farther nodes.

3. 1-D hybrid continuous–discrete multi-node tank model

3.1. Standard 1-D multi-node tank model

Standard 1-D multi-node models found in the literature and commercial software consider heat transfer effects occurring at different levels of the TES tank [38,39]. Fig. 3 illustrates the heat flows observed in the ith node of the tank arising from different heat transfer effects. The rate of change in the sensible heat of the node i ($\dot{H}_i$ [W]) is given by the summation of these heat flows as

$$\dot{H}_i = c_{p,i}\rho_i V_i \dot{T}_i = \dot{Q}_{FC,i} + \dot{Q}_{NC,i} + \dot{Q}_{K,i} - \dot{Q}_{L,i} + \dot{Q}_{G,i} \tag{2}$$

where $c_{p,i}$ [J/(kg °C)] and ρ_i [kg/m^3] are the specific heat capacity and density of water at the node's temperature T_i [°C], and V_i [m^3] is the volume of the node. $\dot{Q}_{FC,i}$ [W] is the heat flow generated by the forced convection heat transfer (i.e. heat transfer generated by the water flow in the tank inlets), $\dot{Q}_{NC,i}$ [W] is the heat flow generated by the natural convection heat transfer, $\dot{Q}_{K,i}$ [W] is the heat flow generated by the conduction heat transfer, $\dot{Q}_{L,i}$ [W] is the heat loss, and $\dot{Q}_{G,i}$ [W] represents the heat flowing into the node from internal or external heat generation sources. In turn, the majority of these heat flows are a function of the temperatures of nodes i, i+1, and i−1—i.e. T_i, T_{i+1} [°C] and T_{i-1} [°C].

The mathematical description of standard 1-D multi-node tank models is presented in detail in Appendix B.

3.2. Flat thermocline in a multi-node tank model

The standard 1-D multi-node modelling approach is susceptible to numerical diffusion [4]. To circumvent this problem and to effectively reproduce the sudden temperature change exhibited by highly thermally stratified TES tanks, two additional considerations were made for the multi-node model. Firstly, an ideal flat thermocline barrier was introduced into the model to predict the vertical position within the tank where the sudden temperature transition occurs. This represents

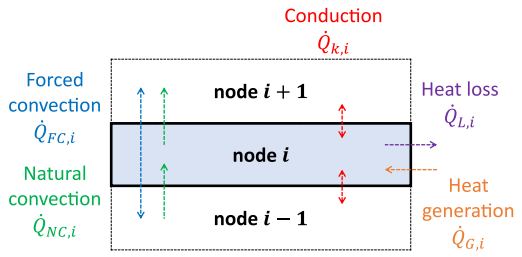

Fig. 3. Heat transfer effects considered in standard 1-D multi-node tank models.

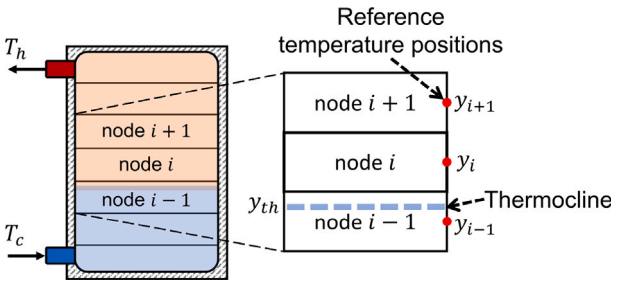

Fig. 4. Multi-node TES tank model with a flat thermocline barrier (dashed blue line) and reference temperature positions (red points).

the thin region between volumes of water with abrupt temperature differences observed in practical TES tanks with a high extent of thermal stratification [10]. Secondly, reference temperature positions on the tank's wall were established at half of the height of each node to determine the location at which the temperature transition is detected in a node.

The flat thermocline barrier is considered ideal in a 1-D flow field. Thus, it is considered to move in plug flow with a uniform velocity distribution in the tank's radial direction. This assumption resembles 1-D representations of a TES tank with an ideal movable insulation baffle [40]. In contrast, two-dimensional (2-D) or 3-D representations must consider the deformation of the thermocline in the tank's radial direction due to the boundary layer generated on the tank wall and other fluid dynamics effects. However, the characterisation of hot water tanks and thermoclines for 2-D and 3-D models falls out of the scope of this paper, which is restricted to 1-D models.

Although the thermocline barrier is considered ideal, it is not considered an adiabatic boundary. Nodes are allowed to exchange heat according to the heat transfer effects described by (2). For example, the difference in temperature exhibited by the nodes directly above and below the flat thermocline barrier increases the conduction heat transfer between the nodes.

Fig. 4 shows the multi-node tank model with a flat thermocline barrier and reference temperature positions, where y_{th} [m] is the vertical position of the thermocline and y_i [m] is the reference temperature position of node i where the transition of T_i is detected. This transition is assumed to happen at half of the height of each node (i.e. 50% of the volume) instead of its borders. This in turn helps maintaining a fixed temperature reference point during charging and discharging processes and reducing the numerical diffusion when calculating the temperature for nodes with large volumes. Thus, an extensive spatial discretisation of the tank is avoided.

In a multi-node tank model, $\dot{Q}_{FC,i}$ and thus $\dot{T}_i$ are dependent on T_{i+1} when charging and instead on T_{i-1} when discharging, as described by Eq. (B.1) in Appendix B. However, in Fig. 4, the flat thermocline barrier represented by the dashed blue line divides node $i-1$ into two zones with a substantial temperature difference between them. Thus, when discharging the tank, the water temperature in node $i-1$ at y_{i-1} (i.e. T_{i-1}) cannot be used to calculate $\dot{T}_i$ until $y_{th} \geq y_i$. Instead, a previous value of T_{i-1}, when $y_{th} < y_{i-1}$, must be considered. In turn, a similar behaviour is expected for calculating $\dot{T}_{i-1}$ using T_i when charging the tank, and the thermocline moves downwards from y_{th} towards y_{i-1}.

The temperature transport phenomenon described above is not time dependent and is determined instead through different discrete events based on y_{th}. This effect is included in the multi-node model as

$$\dot{Q}_{FC,i} = \begin{cases} c_{p,i}\rho_i \dot{V}_{in}(T_{i+1,k} - T_i) & \forall\ \dot{V}_{in} > 0 \\ c_{p,i}\rho_i \dot{V}_{in}(T_i - T_{i-1,k}) & \forall\ \dot{V}_{in} < 0 \end{cases} \tag{3}$$

where $\dot{V}_{in}$ [m^3/s] is the volumetric water flow induced through the tank's inlets and crossing node i, and $T_{i+1,k}$ [°C] and $T_{i-1,k}$ [°C] are discrete temperature values for nodes $i+1$ and $i-1$ at a discrete moment k, which may be different than temperatures T_{i+1} and T_{i-1}. The discrete temperature value of node j is periodically updated based on the position of the thermocline for the next discrete moment $k+1$ ($y_{th,k+1}$) when $\dot{V}_{in} > 0$ as

$$T_{j,k+1} = \begin{cases} T_j & \forall\ y_{th,k+1} > y_j \vee y_{th,k+1} < y_{j-1} \\ T_{j,k} & \forall\ y_j < y_{th,k+1} < y_{j-1} \end{cases} \tag{4}$$

and when $\dot{V}_{in} < 0$ as

$$T_{j,k+1} = \begin{cases} T_j & \forall\ y_{th,k+1} > y_{j+1} \vee y_{th,k+1} < y_j \\ T_{j,k} & \forall\ y_{j+1} < y_{th,k+1} < y_j \end{cases} \tag{5}$$

The value of $y_{th,k+1}$ is updated as

$$y_{th,k+1} = y_{th,k} - v_{th,k}\Delta t \tag{6}$$

where $v_{th,k}$ [m/s] is the vertical linear velocity of the thermocline given by the volumetric flow divided by the cross-sectional area of the tank A_c [m^2] ($v_{th,k} = \dot{V}_{in}/A_c$), and Δt [s] is the constant time step between k and $k+1$.

3.3. Flat thermocline formation during charging or discharging only

As discussed in Section 2.1, the control configuration of heat sources and sinks may produce a different extent of thermal stratification for charging and discharging operations of hot water tanks. For a tank presenting a thin thermocline during charging or discharging only, the dynamics of the multi-node tank model described by (3)–(6) must be modified accordingly. For example, for a thin thermocline present during charging only, the sudden transition of temperature does not occur when the tank is discharged. Therefore, the discrete temperature value of node j can be approximated to its continuous value during discharging, and (5) is simplified to $T_{j,k+1} = T_j$. In this scenario, the thin thermocline barrier is destructed during discharging and formed again when charging the tank. Thus, y_{th} is updated as

$$y_{th,k+1} = \begin{cases} y_{th,k} - v_{th,k}\Delta t & \forall\ \dot{V}_{in} > 0 \\ y_{hin} & \forall\ \dot{V}_{in} < 0 \end{cases} \tag{7}$$

where y_{hin} [m] is the vertical position of the hot inlet. Conversely, for a thin thermocline present during discharging only, (4) is simplified to $T_{j,k+1} = T_j$ and y_{th} is updated as

$$y_{th,k+1} = \begin{cases} y_{cin} & \forall\ \dot{V}_{in} > 0 \\ y_{th,k} + v_{th,k}\Delta t & \forall\ \dot{V}_{in} < 0 \end{cases} \tag{8}$$

where y_{cin} [m] is the vertical position of the cold inlet.

3.4. Simulation of hybrid continuous–discrete systems

Fig. 5 shows the mathematical model of a hybrid continuous–discrete time system such as the one presented in the previous subsections, where the output vector **y** is determined from the input vector **u**

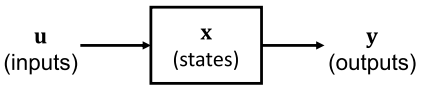

$$\mathbf{y} = f_o(t, \mathbf{x}, \mathbf{u})$$
$$\dot{\mathbf{x}}_c = f_d(t, \mathbf{x}, \mathbf{u})$$
$$\mathbf{x}_{d_{k+1}} = f_u(t, \mathbf{x}, \mathbf{u})$$
$$\mathbf{x} = [\mathbf{x}_c \quad \mathbf{x}_d]$$

Fig. 5. Hybrid continuous–discrete system [41].

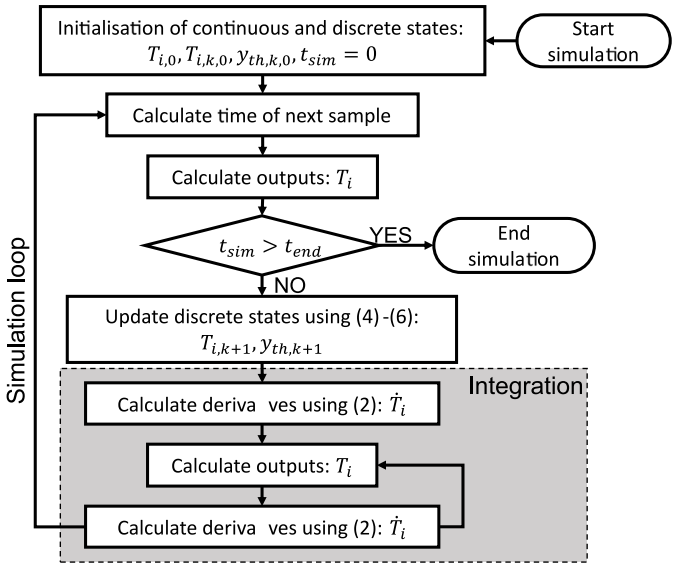

Fig. 6. Simulation process of the hybrid continuous–discrete multi-node tank model in MATLAB/Simulink [41].

and a combination of continuous and discrete states $\mathbf{x}_c$ and $\mathbf{x}_d$. For a tank model with N nodes, these vectors are defined as

$$\mathbf{u} = [T_{in} \quad \dot{V}_{in}] \tag{9}$$

$$\mathbf{y} = \mathbf{x}_c = [T_1 \quad T_2 \quad \cdots \quad T_N]^{\mathrm{T}} \tag{10}$$

$$\mathbf{x}_d = [T_{1,k} \quad T_{2,k} \quad \cdots T_{N,k} \quad y_{th,k}]^{\mathrm{T}} \tag{11}$$

where T_{in} is defined as the charging and discharging inlet temperatures T_c [°C] and T_h [°C] in (B.2) and (B.3) in Appendix B. $\mathbf{x}_c$ is obtained by calculating the integral of the continuous states' derivative $\dot{\mathbf{x}}_c$, and $\mathbf{x}_d$ is updated for the next discrete moment $k+1$ ($\mathbf{x}_{d_{k+1}}$). In turn, $\dot{\mathbf{x}}_c$ is given by (2) and $\mathbf{x}_{d_{k+1}}$ is given by (4) to (6). The update of the discrete states is carried out in a time step Δt which is larger than the time step used in the integration of the derivatives of the continuous states, but that is sufficiently small to capture the thermocline transport phenomenon.

System-functions (S-functions) available in MATLAB/Simulink constitute a powerful tool to implement and simulate these hybrid systems in programming languages such as C, C++, Fortran and MATLAB [41]. Fig. 6 shows the simulation process in MATLAB/Simulink of the hybrid continuous–discrete multi-node tank model presented in Section 3.2.

The model implementation and the computational simulations reported in the paper were carried out using MATLAB/Simulink, as this software enables to implement the hybrid continuous–discrete time system models required for the modelling approach presented in this section. For the sake of simplicity of testing and comparison, the 1-D standard models of water tanks were also programmed in MATLAB using the multi-node modelling approach described in Appendix B.

4. Description and modelling of the experimental facility

4.1. Experimental facility

The modelling approach presented in Section 3 was experimentally validated using the heat storage system reported in [42]. Experiments for charging and discharging a TES tank were performed using a combination of a condensing boiler and a heat sink, as shown in Fig. 7.

The experimental facility incorporates a Wolf BSP-800 TES tank with a water capacity of 785 l (see Fig. 8(a)) [43]. Temperature was measured using ten PT100 sensors evenly distributed over the height of the tank's wall (between the outside wall and the thermal insulation cover) to determine its internal temperature profile. Temperature sensors were installed as immersion sensors in the supply and return pipelines at each terminal of the tank, the condensing boiler and the heat sink—i.e. eight sensors in total. Charging and discharging flows were measured with electromagnetic flow meters, as shown in Fig. 7.

A Wolf CGB-2/20 20-kW condensing boiler [44] was used to supply heat to charge the tank. The boiler was operated at its maximum heat power during the experiment. Its internal control was set to maintain a constant temperature difference of 20 °C between supply and return.

Heat consumption was emulated by a parallel-flow heat exchanger in the heat sink. By using a mixer in its primary side, the temperature of the water flow supplied to the heat exchanger may be regulated (e.g. 40 °C for an underfloor heating system or 65 °C for a radiator). A controllable pump in the primary side provided the desired flow rate. The cooling water flow in the secondary side of the heat exchanger (purple pipelines in Fig. 7) was regulated with a control valve to obtain a desired return temperature of the heating system. In turn, this temperature is also the discharging temperature of the tank. The experiment was run with a set return temperature from the heating system of 30 °C.

4.2. Modelling of the TES tank

According to the datasheet of the TES tank [43], this was modelled as a cylindrical 1-D multi-node tank with a height of 1755 mm and a diameter of 790 mm (see Fig. 8(b)). The model considers 12 layers, numbered from 0 to 11 from bottom to top. The height of each tank layer is 150 mm for layers 1 to 11 and 105 mm for layer 0. Each layer may be discretised into a number of nodes to increase the spatial resolution of the model. For instance, a resolution of 5 nodes per layer results in a 60-node tank model. The height of the PT100 sensors within the tank coincides with the centre of layers 1 to 10, as shown in Fig. 8(b).

The condensing boiler and the heat sink are connected to the lowest and highest main inlets of the tank located at a height of 260 mm and 1430 mm from the bottom, respectively (see Fig. 8(a)). Thus, hot water is injected and subtracted directly from layer 9 of the tank and cold water from layer 2 (see Fig. 8(b)). The water flow is considered ideal at the inlets of the tank for a 1-D model. This implies that the horizontal volumetric flow entering and exiting the tank through the inlets is assumed vertical from the inlet to the outlet. Therefore, layers 2 to 9, located between the inlets and outlets of the tank, present heat transfer by forced convection, while layers 0, 1, 10 and 11 are dead volumes.

The condensing boiler and heat sink are connected to the tank via 1.5-inch threads and insulated pipelines with a diameter of 22 mm, circulating water through the tank using hydraulic pumps. However, neither the condensing boiler nor the heat sink are represented in the simulation model. Instead, their effect is inherently present in the charging and discharging flow and temperature conditions for the tank adopted from the experimental test and measured at the tank inlets.

The TES tank was modelled in MATLAB/Simulink using the 1-D hybrid continuous–discrete multi-node modelling approach introduced

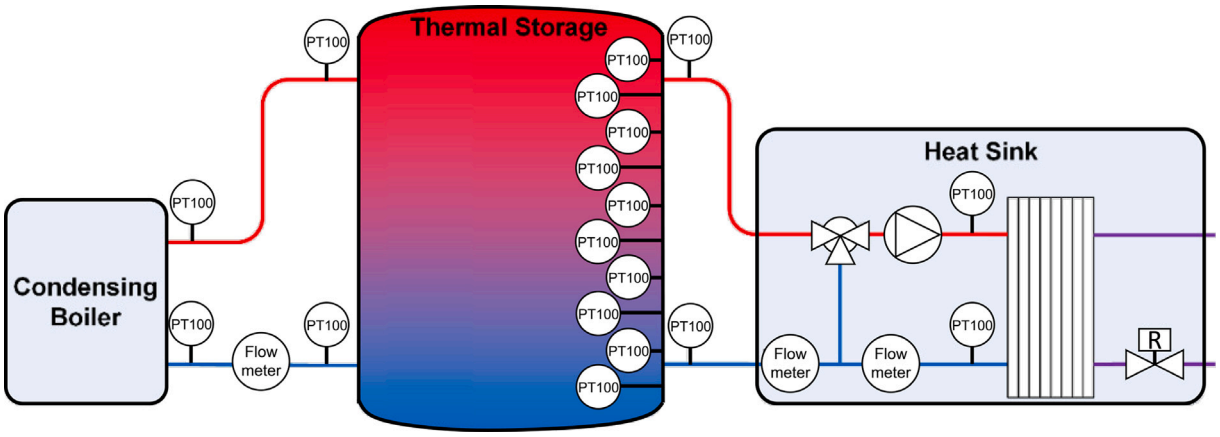

Fig. 7. Experimental setup with a condensing boiler, TES unit and heat sink connected through supply (red) and return (blue) pipelines.

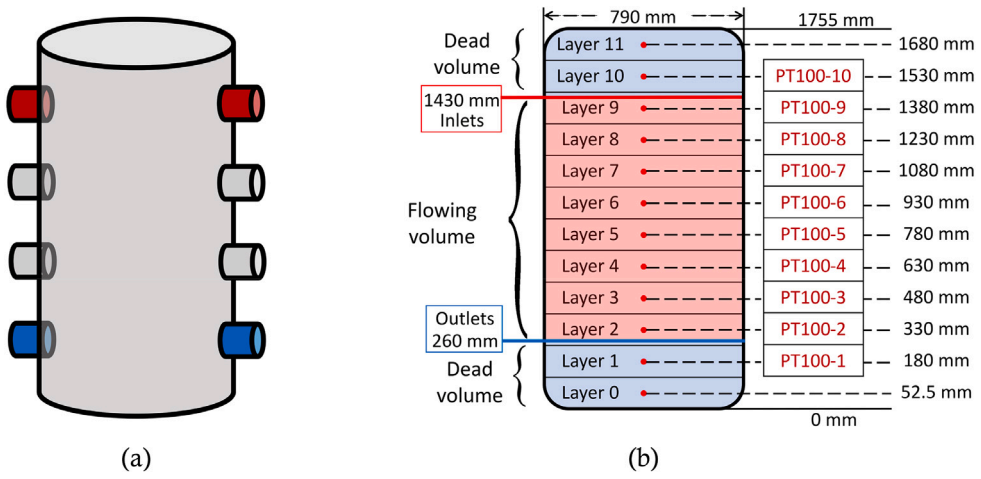

Fig. 8. (a) Side inlets of the Wolf BSP-800 heat storage tank (red and blue inlets), and (b) multi-node tank model. (**Note**: Although the storage tank has further inlets and an internal heat exchanger, none of these were used to charge or discharge the tank.).

in Section 3 to characterise its dynamics. To corroborate the effectiveness of the hybrid multi-node model, this was compared against the standard multi-node models often used in the literature and adopted by commercial software (see Appendix B). Thus, three different tank models were assessed:

- A standard multi-node tank model with a spatial resolution of 1 node per layer, here termed standard 12-node model.
- A standard multi-node tank model with a spatial resolution of 5 nodes per layer, here termed standard 60-node model.
- A hybrid continuous–discrete multi-node tank model with a spatial resolution of 1 node per layer and $\Delta t = 1$ s, here termed hybrid 12-node model.

4.3. Heat losses

Heat losses in the tank were modelled using (B.10) and (B.11) for all models, as described in Appendix B. The heat loss transfer coefficient due to forced convection $U_{FC,i}$ [W/(m^2 °C)] was obtained according to the flow regime, as shown in [45], and the heat loss transfer coefficient for the tank's standby condition $U_{0,i}$ [W/(m^2 °C)] was experimentally characterised for each layer of the tank model as described in Appendix C. Values of $U_{0,i}$ for each tank layer are shown in Table C.1. The resulting $\dot{Q}_{L,i}$ in each layer of the tank was equally distributed to all the layer's nodes in the case of the standard 60-node tank model (i.e. $\dot{Q}_{L,i}/5$).

5. Experimental validation

5.1. Experimental and simulation conditions

The hybrid 12-node model was experimentally validated for a complete charging and discharging cycle of the storage tank. This was performed in a single trial and under practical operational conditions.

The tank was charged from an initial fully discharged condition (SoC = 0%) at an ambient temperature of 20 °C up to 60 °C. Although the storage tank can be charged up to a maximum temperature of around 85 °C, 60 °C was deemed sufficient to avoid overspending energy when conducting the experiment. This is because reaching 85 °C during charging does not contribute to achieving a higher thermal stratification or producing a thin thermocline due to the condensing boiler's operation. Charging limitations are discussed further in Section 5.2. The tank was later discharged at a constant discharging temperature T_c = 30 °C, as this temperature is commonly observed in the return pipeline of practical domestic heating systems for space conditioning [46,47].

The duration of the charging and discharging processes of the storage tank depends on the value of $\dot{V}_{in}$. In turn, this depends on the operation of the condensing boiler and the heat sink, described in Section 4.1. Thus, the storage tank was charged for three hours and discharged in the subsequent two hours of the experiment.

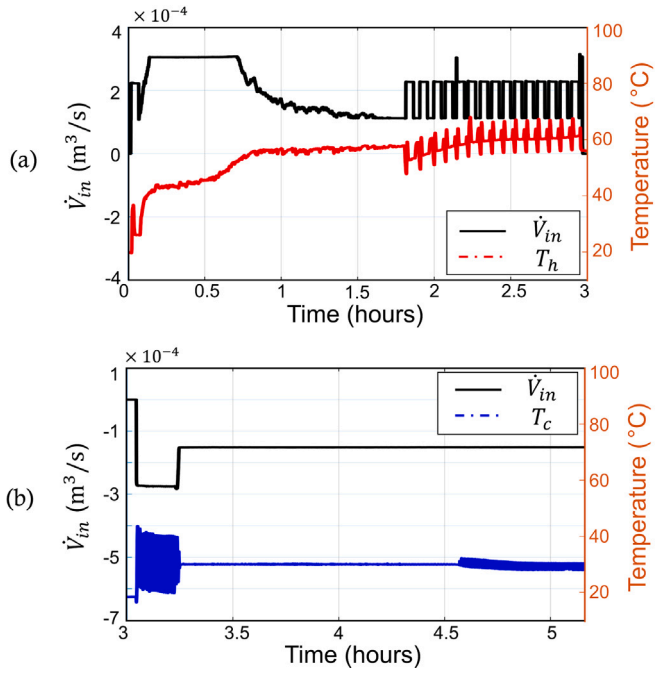

Fig. 9. Experimental flow and temperature conditions during: (a) charging and (b) discharging.

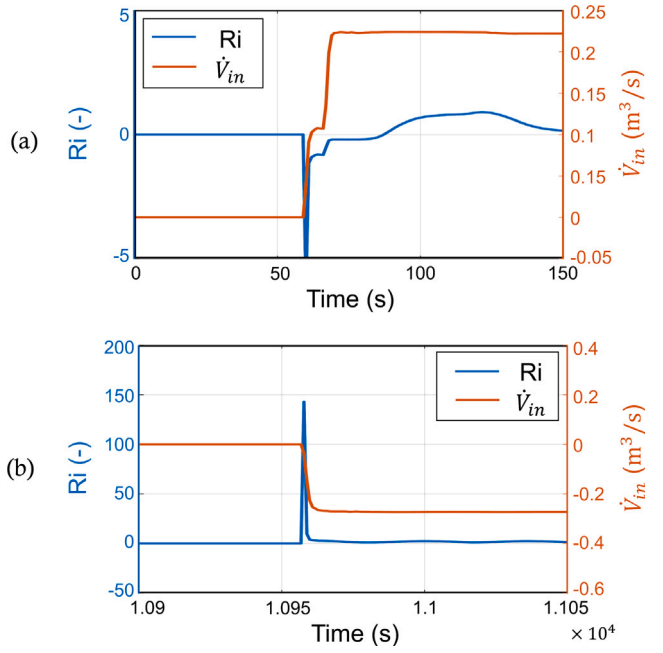

Fig. 10. Variation of Richardson's number during the first two minutes of the (a) charging and (b) discharging experiments. The inlet volumetric flow rate was included to identify the beginning of the experiments.

Simulations of the TES tank were carried out considering similar charging and discharging flow and temperature conditions during the experiments. Fig. 9(a) shows the experimental measurements for $\dot{V}_{in}$ and T_h for charging, while Fig. 9(b) shows the measurements of $\dot{V}_{in}$ and T_c for discharging. T_h and T_c were measured by the PT100 sensors in the boiler's supply pipeline and the sink's return pipeline, respectively—with both sensors placed at the tank's terminals. On the other hand, $\dot{V}_{in}$ was measured by the flow meters in the return pipelines connected to the TES tank (see Fig. 7).

5.2. Thermocline considerations

Due to the limitations of the condensing boiler and the heat sink to strictly control the charging and discharging temperatures and the additional standby heat losses in the connection pipelines, the transient behaviours of T_h and T_c were substantially impacted. Although these variations impact the thermal stratification and formation of the thermocline by generating mixing within the tank, the charging process was primarily affected.

Fig. 10 shows the variations of the Richardson's number during the first two minutes of the charging and discharging experiments. Ri is given by (1), where u_{in} is calculated considering an inlet diameter $D_{in} = 0.0381$ m ($u_{in} = 4|\dot{V}_{in}|/\pi D_{in}^2$) and a T_{st} equal to the temperature measured by the nearest PT100 sensor to the tank inlet (i.e. PT100-9 for charging and PT100-2 for discharging). The initial negative values of Ri during charging indicate the temporal inversion of thermal stratification (i.e. colder water injected above a hot medium) and the generation of mixing at the inlet of the tank. Conversely, the high positive values of Ri followed by its rapid settlement during the tank's discharging suggest a highly stable thermal stratification and the formation of a thin thermocline. Considering these characteristics, the thermocline position in the hybrid 12-node tank model was updated using (8).

5.3. Verification of temperatures and SoC

The spatial resolution adopted for the standard 12-node, standard 60-node and hybrid 12-node tank models ensures each PT100 sensor in the experimental configuration coincides with the centre of a node. This facilitates a direct comparison between the experimental measurements and simulated temperatures. The temperatures of the layers between the hot and cold inlets of the tank (i.e. layers 2 to 9), were compared. To this end, the root mean square error (RMSE) and the mean absolute error (MAE) between simulation and experimental results were obtained for the three models. For the standard 60-node model, the RMSE and MAE were calculated for the temperature of the central node of the tank layers. These errors are expressed as

$$\mathrm{RMSE} = \sqrt{\frac{1}{n}\sum_{a=1}^{n}(\hat{z}_a - z_a)^2} \tag{12}$$

$$\mathrm{MAE} = \frac{1}{n}\sum_{a=1}^{n}|\hat{z}_a - z_a| \tag{13}$$

where $\hat{z}_a$ and z_a are specific samples of the model and experimental measurements, and n the total number of samples.

A more practical comparison was conducted for the SoC of the tank. For a hot water TES tank model with N nodes, the SoC was calculated from temperature measurements as

$$\mathrm{SoC} = \frac{(\sum_{i=1}^{N} c_{p,i}\rho_i V_i T_i) - c_{p,min}\rho_{min}V_{st}T_{min}}{c_{p,max}\rho_{max}V_{st}T_{max} - c_{p,min}\rho_{min}V_{st}T_{min}} \times 100 \tag{14}$$

where T_{min} [°C] and T_{max} [°C] are the minimum and maximum operating temperatures in the tank and V_{st} [m^3] is the total volume of the storage tank. For the BSP-800 tank, $T_{min} = 20$ °C and $T_{max} = 85$ °C. This implies that SoC = 100% for a uniformly distributed temperature of 85 °C in the tank. The actual SoC of the tank was calculated from experimental measurements using (14), discretising the tank into 12 layers, as shown in Fig. 8(b), and assuming layers 11 and 0 exhibit the same temperatures measured by PT100 sensors in layers 10 and 1, respectively. The RMSE and MAE of the SoC were also calculated.

5.4. Comparison between simulation and experimental results

Fig. 11 shows the comparison between simulation and experimental results for a charging and discharging cycle of the TES tank. The

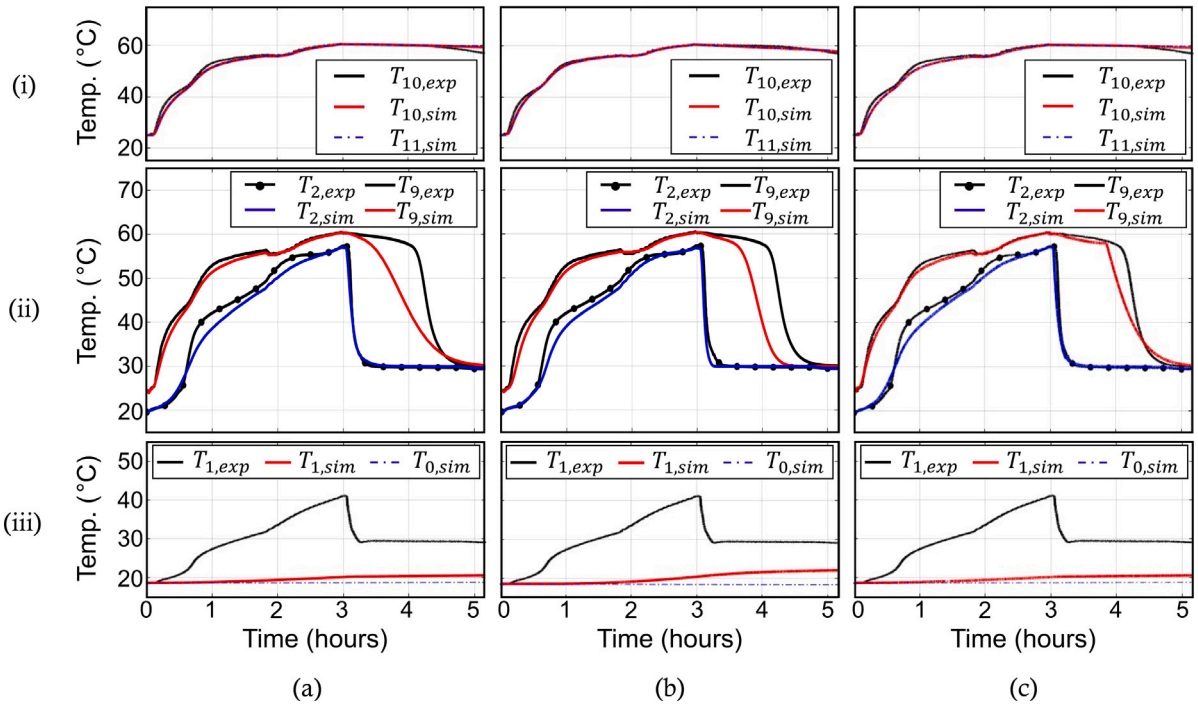

Fig. 11. Experimental and simulation measurements of layer temperature for (a) standard 12-node model, (b) standard 60-node model and (c) hybrid 12-node model. Plots in (i) show the temperature measurements for layers 10 and 11, (ii) for layers 2 and 9, and (iii) for layers 0 and 1.

tank is charged during the first three hours into the simulations and discharged in the following two hours. Temperature measurements from experiments are identified as $T_{l,exp}$, where subscript 'l' denotes the number of the layer coinciding in height with a respective PT100 sensor. Temperatures from simulations are identified as $T_{l,sim}$.

The three simulated tank models exhibit similar temperature profiles during the charging process (first three hours in Fig. 11). However, different temperature profiles are observed during discharging for layers 2 to 9 (final two hours in Fig. 11a–ii, b–ii and c–ii). Differences are especially noticeable in the simulated temperature of layer 9 ($T_{9,sim}$, red trace) with respect to $T_{9,exp}$ (black trace), which exhibits a sudden transition from 60 °C to 30 °C during discharging. Instead, the standard 12-node tank model exhibits a smooth transition of $T_{9,sim}$ due to the inherent artificial numerical diffusion (see Fig. 11a-ii). Although $T_{9,sim}$ captures the sudden temperature transition for the standard 60-node tank model, this occurs sooner than for the experimental process (see the trace of $T_{9,exp}$ in Fig. 11b-ii). The hybrid 12-node tank model captures the delayed transition in $T_{9,sim}$ and thus achieves a better agreement with $T_{9,exp}$ (see Fig. 11c-ii) than the standard models as the thermocline transport phenomenon was considered.

Temperature measurements in the top and bottom dead volumes of the tank exhibit a similar behaviour for the three models (see plots (i) and (iii) in Fig. 11) and achieve a good agreement with $T_{10,exp}$ (black trace in plots (i)). However, none of the models predicts accurately the behaviour of $T_{1,exp}$ (black trace in plots (iii)). $T_{1,exp}$ substantially increased to 40 °C during charging and rapidly converged to $T_c = 30$ °C during discharging. Although the behaviour of $T_{10,exp}$ can be explained by the presence of natural convection heat transfer when the tank is charged at a higher temperature (as described in Appendix B), this is not the case for $T_{1,exp}$, which also increases during charging.

The lack of accuracy between $T_{1,exp}$ and $T_{1,sim}$ (black and red traces in plots (iii) of Fig. 11) may be caused by the deformation of the water stream at the cold inlet during the charging process, which generates unexpected and unwanted mixing flows with the adjacent dead volume. Possible causes of this turbulence may be the immersed helical heat exchanger opposing the water stream within the tank [48,49], or the generation of a "vena contracta" produced by "free jet" conditions at the bottom of the tank and the geometry of the inlets, which is common in vertical containers [50]. To avoid inlet mixing and enhance thermal stratification in hot water tanks, dead zones must be minimised [51].

The analysis of water stream deformations may require 2-D or 3-D CFD simulations, which falls out of the scope of this work as this is limited to 1-D models. Thus, the relative accuracy between 1-D models is restricted to that afforded by estimating the temperatures of the intermediate layers (i.e. $T_{2,sim}$ and $T_{9,sim}$ given by the blue and red traces), shown in plots (ii).

Overall, simulation results from the hybrid 12-node model exhibit a better agreement with experimental results than the standard 12-node and standard 60-node models. This is a consequence of the reduced numerical diffusion in the hybrid model resulting from incorporating the variable for the position of the thermocline in the calculation of the temperature transition of the intermediate layers generated by forced convection heat transfer.

Fig. 12 shows a comparison of the temperature measurements in the intermediate layers of the tank models with respect to the experimental measurements (solid black traces). For the standard and hybrid 12-node models, which have a spatial resolution of 1 node per layer, only one temperature is displayed for each layer (dashed blue and solid red traces, respectively). On the other hand, five temperatures are displayed for the standard 60-node model, which correspond to the temperatures of each node within the layer (solid green traces). The top and bottom nodes of each layer of the standard 60-node model present a temperature difference with respect to the temperature of the central node, with maximum differences of 3.5 °C and 10.8 °C in layers 9 and 2 during the discharging. Although the layer temperatures converge with the experimental measurements for the standard and hybrid models during the charging of the storage tank, a gradual and significant deterioration in the accuracy of both standard models is observed during discharging from lower to upper layers. Such a deterioration is not as dramatic in the hybrid model.

Fig. 13 shows the SoC variation through charging and discharging of the tank for all simulation models and experimental data. The SoC calculation was done using (14). Based on the results presented in Fig. 11, the three models exhibit a similar SoC transition during

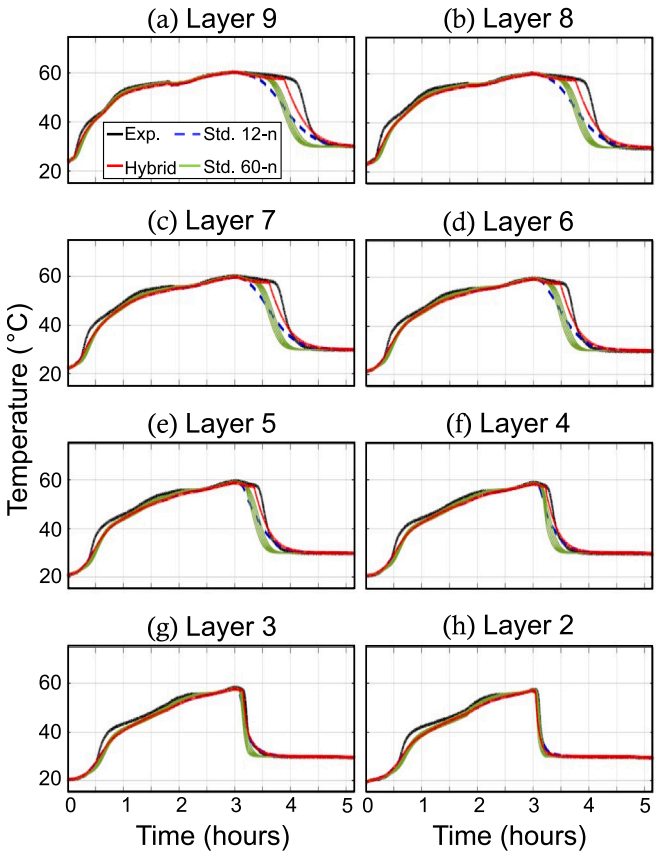

Fig. 12. Experimental (solid black traces) and simulation temperature measurements for the intermediate layers of the standard 12-node model (dashed blue traces), standard 60-node model (light green traces) and the hybrid 12-node model (red traces).

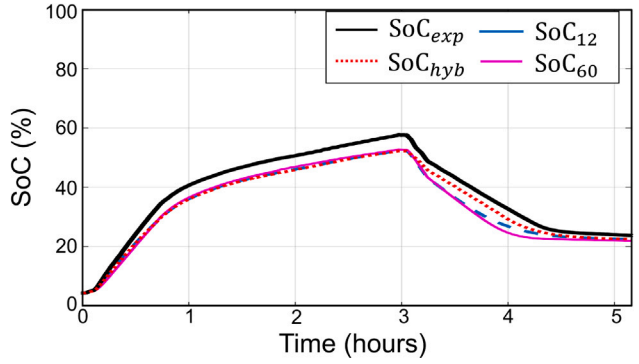

Fig. 13. Comparison of the SoC calculated for the standard 12-node (SoC$_{12}$), standard 60-node (SoC$_{60}$), and hybrid 12-node (SoC$_{hyb}$) models against the SoC obtained from experimental measurements (SoC$_{exp}$).

charging but diverge during discharging. The SoC of the hybrid 12-node model (SoC$_{hyb}$) exhibits a better agreement with the SoC obtained from experimental data (SoC$_{exp}$) during discharging. However, the SoC obtained from the models progressively diverges from SoC$_{exp}$ due to the temperatures exhibited at the bottom of the tank—i.e. $T_{1,sim}$ and $T_{0,sim}$.

A modified SoC (SoC$_m$) was calculated using (14) and excluding T_{10} to compare the simulation with experimental results without considering the effects of turbulence at the bottom dead zone of the tank. Fig. 14 shows the modified SoC for each tank model and the real tank. As it can be observed, the hybrid 12-node model accurately predicts the SoC of the real TES tank during the complete charging and discharging cycle.

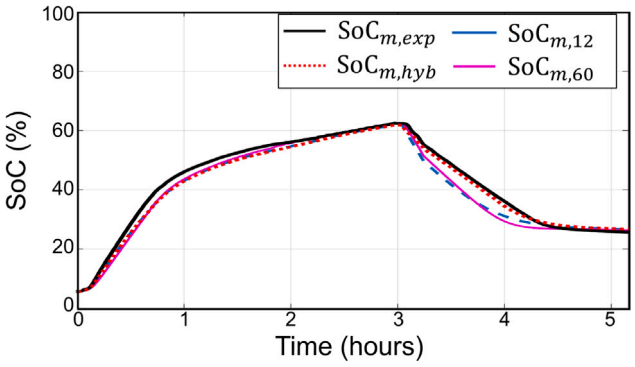

Fig. 14. Comparison of the SoC$_m$ calculated for the standard 12-node (SoC$_{m,12}$), standard 60-node (SoC$_{m,60}$), and hybrid 12-node (SoC$_{m,hyb}$) models with the SoC$_m$ obtained from experimental measurements (SoC$_{m,exp}$).

To quantitatively assess the outcomes of the simulation models, Tables 1 and 2 show the RMSE and MAE of the standard 12-node, standard 60-node, and hybrid 12-node models for the temperatures in layers 2 to 9 (T_2 to T_9) during the complete charging and discharging cycle of the tank. In turn, these errors were also calculated for the individual charging and discharging cycles. Similarly, the RMSE and MAE of the SoC and SoC$_m$ are shown in Table 3 for the three models.

For the charging cycle, the three models have a similar accuracy for all the parameters, with the standard 60-node model producing in general slightly smaller errors for T_2 to T_5, SoC and SoC$_m$, and larger errors for T_6 to T_9. However, for the discharging cycle, the hybrid 12-node model reduces the RMSE and MAE of T_3 to T_9 with respect to the standard models. For T_9, the hybrid 12-node model considerably reduces the RMSE in 3.9 °C and MAE in 2.84 °C with respect to the standard 12-node model—clearly outperforming it. The hybrid model also decreases the RMSE of the SoC and SoC$_m$ in 1.9% and 2.83%, and their MAE in 1.49% and 2.04% compared to the standard 12-node model. Notably, the standard 60-node model produces the largest errors for T_2 to T_9 and SoC during the discharging cycle and consequently during the estimation for the complete charging and discharging cycle, regardless of its higher spatial resolution.

6. Discussion on the limitations of the hybrid modelling approach

6.1. Deformations of the water stream within the TES tank

Although the 1-D hybrid continuous–discrete model presented in this paper proved highly effective for simulating the thermal dynamics of a real hot water TES tank, certain limitations must be considered when implementing the modelling approach.

In the first instance, mixing phenomena generated by water stream deformations within the tank are not modelled, neither by the hybrid continuous–discrete model nor by standard models. This limitation is inherent of the 1-D tank models, with flow deformations produced by the boundary layers adjacent to the inner wall of the tank and pipes not being included. Flow deformations can also be produced within the dead volumes due to the tank inlet and outlet positions, leading to substantial simulation errors, as observed in Fig. 11a–iii, b–iii and c–iii. Consequently, reducing the dead volume within the tank is highly recommended by placing the inlets as close as possible to the top and bottom of the tank [51].

Charging and discharging temperature and flow conditions can also generate deformations of the water stream in the inlets of the TES tank due to natural convection. Buoyant forces acting on water streams injected horizontally into the tank may cause the formation of buoyant jets and vortices, thus deteriorating the thermal stratification [52]. Although the Richardson's number offers a practical insight into the

Table 1
RMSE of the standard 12-node (Std. 12), standard 60-node (Std. 60), and hybrid 12-node (H. 12) models for T_2 to T_9.

Test	Model	Layer temperature [°C]							
		T_2	T_3	T_4	T_5	T_6	T_7	T_8	T_9
Charging and discharging	Std. 12	1.67	2.07	2.65	3.36	3.72	4.19	4.58	4.94
	Std. 60	2.06	2.55	3.35	4.08	4.49	5.05	5.54	6.03
	H. 12	1.68	1.39	1.48	1.69	1.74	1.97	2.28	2.45
Charging	Std. 12	1.7	1.66	1.50	1.59	1.39	1.40	1.40	0.72
	Std. 60	1.57	1.60	1.46	1.58	1.42	1.47	1.57	0.88
	H. 12	1.72	1.67	1.51	1.61	1.41	1.42	1.42	0.73
Discharging	Std. 12	1.65	2.56	3.74	4.90	5.57	6.32	6.96	7.66
	Std. 60	2.62	3.51	4.93	6.09	6.81	7.68	8.45	9.35
	H. 12	1.65	0.88	1.44	1.82	2.14	2.56	3.14	3.73

Table 2
MAE of the standard 12-node (Std. 12), standard 60-node (Std. 60), and hybrid 12-node (H. 12) models for T_2 to T_9.

Test	Model	Layer temperature [°C]							
		T_2	T_3	T_4	T_5	T_6	T_7	T_8	T_9
Charging and discharging	Std. 12	1.01	1.13	1.37	1.72	1.89	2.17	2.40	2.37
	Std. 60	1.11	1.35	1.59	2.02	2.10	2.44	2.67	2.74
	H. 12	1.03	0.96	1.05	1.16	1.15	1.26	1.39	1.21
Charging	Std. 12	1.34	1.29	1.16	1.24	1.03	1.07	1.05	0.55
	Std. 60	1.08	1.11	1.00	1.10	0.95	1.00	1.05	0.55
	H. 12	1.36	1.30	1.17	1.26	1.05	1.09	1.07	0.57
Discharging	Std. 12	0.57	0.92	1.69	2.42	3.14	3.76	4.38	4.98
	Std. 60	1.17	1.72	2.44	3.36	3.79	4.54	5.01	5.88
	H. 12	0.6	0.48	0.89	1.05	1.32	1.53	1.88	2.14

Table 3
RMSE and MAE of the standard 12-node (Std. 12), standard 60-node (Std. 60), and hybrid 12-node (H. 12) models for SoC and SoC_m.

Test	Model	RMSE		RMSE	
		SoC [%]	SoC_m [%]	SoC [%]	SoC_m [%]
Charging and discharging	Std. 12	4.5	2.8	4.04	2.04
	Std. 60	4.86	3.64	4.34	2.46
	H. 12	3.52	1.41	3.25	1.22
Charging	Std. 12	3.88	1.57	3.64	1.32
	Std. 60	3.44	1.55	3.31	1.15
	H. 12	4.61	1.59	4.33	1.35
Discharging	Std. 12	5.21	3.95	4.55	3.11
	Std. 60	6.35	5.37	5.78	4.37
	H. 12	3.31	1.12	3.06	1.07

inlet conditions, as shown in Section 5.2, these conditions must be effectively controlled every time the tank is charged or discharged to guarantee the formation of a thin thermocline—thus ensuring the applicability of the hybrid continuous–discrete modelling approach. In addition, there is not a minimum value of Richardson's number that indicates the generation of a flat thermocline.

6.2. Transitions between high and low thermal stratification conditions

The inclusion of the thermocline displacement effect in the presented hybrid continuous–discrete modelling approach allows simulating, with an enhanced accuracy, practical TES tanks exhibiting a high extent of thermal stratification during charging and discharging operations. However, transitions between high and low thermal stratification conditions are not represented. Variations in the operating temperature and flow conditions between charging and discharging cycles may generate mixing at the tank's inlets, deteriorating the thermal stratification in the tank and leading to a reduced accuracy.

To support this argument, Ref. [7] is considered, where the thermal stratification of a 128 l hot water tank with 8 temperature sensors was assessed for different inlet configurations and discharging flow rates. The tank was discharged from an initial uniform temperature of 60 °C with flow rates of 5, 10 and 15 lpm at 15 °C. It is shown in the reference that a slotting-type inlet reduces the mixing at the tank, enhancing its thermal stratification. However, as the discharging flow rate increases, the thermal stratification deteriorates due to mixing.

Fig. 15 shows a comparison of the experimental results reported in [7] for discharging processes at different flow rates, as described in the previous paragraph, with the simulation results obtained with standard and hybrid 8-node models. Thus, there is a spatial resolution of 1 node per layer in both models. In the figure, temperature measurements from layers 1, 5 and 8 are shown, denoted by subscripts '1', '5' and '8'. Subscripts 'exp', 'std' and 'hyb', denote, respectively, experimental data, results from the standard model, and results from the hybrid model. For flow rates at 5 and 10 lpm shown in Fig. 15(a) and (b), respectively, the hybrid 8-node model achieves the best match for all layers except for layer 8, with both models achieving a similar performance. However, for a flow rate of 15 lpm (see Fig. 15(c)), the standard 8-node model achieves the best match as the thermal stratification is the lowest for any of the experiments.

6.3. Trade-off between model accuracy and simulation speed

Another limitation to consider when choosing a modelling approach is the trade-off between the accuracy of simulation results and the model's computational expense. Although the 1-D hybrid continuous–discrete tank model produces more accurate simulation results, estimating the position of the thin thermocline and updating the discrete states

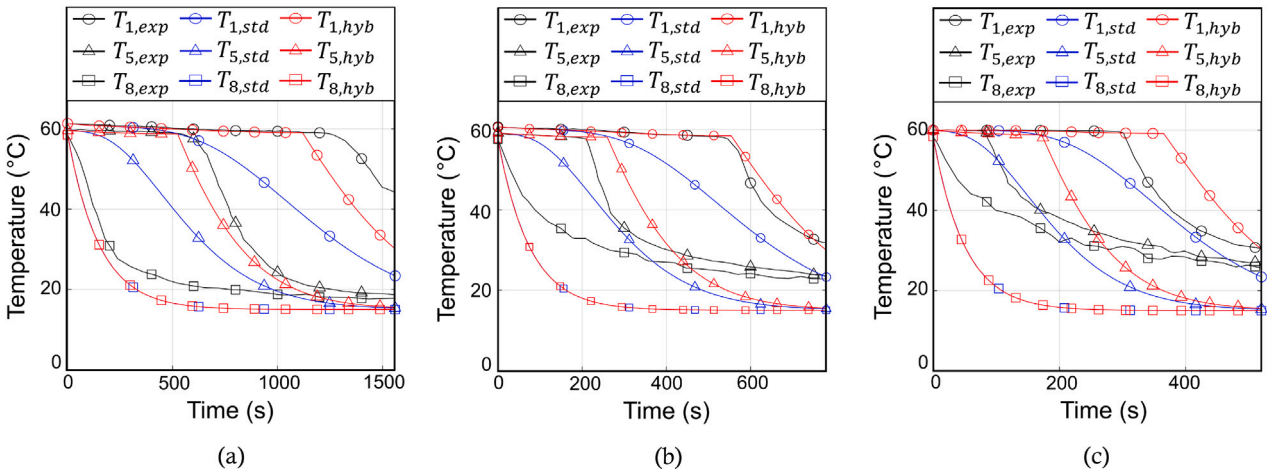

Fig. 15. Comparison of the experimental results obtained for the hot water tank reported in [7] with the simulation results from standard and hybrid 8-node tank models for discharging flows of (a) $\dot{V}_{in} = 5$ lpm, (b) $\dot{V}_{in} = 10$ lpm and (c) $\dot{V}_{in} = 15$ lpm.

Table 4
Simulation time ratios obtained from simulating the standard 12-node, standard 60-node, and hybrid 12-node models for a complete charging and discharging cycle.

Model	Simulation time ratio
Standard 12-node	0.0015
Standard 60-node	0.07
Hybrid 12-node	0.03

Table 5
Simulation time ratios obtained from simulating the hybrid 12-node model for different Δt.

Δt [s]	Simulation time ratio
1	0.03
5	0.005
10	0.0042

result in larger simulation times than for 1-D standard tank models with similar spatial resolutions.

Table 4 shows a comparison of the simulation time ratios (i.e. real-time seconds per one second of simulation) obtained for the standard 12-node, standard 60-node, and hybrid 12-node models. As it can be observed, the simulation of the standard 12-node model is twenty times faster than for the hybrid 12-node model. However, the simulation of the hybrid 12-node model is two times faster than the simulation of the 60-node model.

The simulation time ratio of the hybrid 12-node model can be enhanced by increasing Δt for updating its discrete states. However, this is achieved at the cost of a reduced accuracy of the model. Table 5 presents a comparison of the simulation time ratios obtained for a complete charging and discharging cycle of the hybrid 12-node tank model for different Δt. Tables 6, 7 and 8 present a comparison of the RMSE and MAE for T_2 to T_9, SoC and SoC_m obtained from the simulations. Although the simulation time was substantially reduced as Δt increased from 1 to 10 s (see Table 5), the RMSE and MAE of T_2 to T_9, SoC and SoC_m increased for the discharging process of the tank (see Tables 6 to 8).

7. Conclusions

Accurate yet simple 1-D dynamic models are required to predict and analyse the behaviour of the thermal gradient within hot water TES tanks and, in turn, effectively calculate their SoC. Standard multi-node models with a high spatial resolution (i.e. high number of nodes) have been normally adopted to simulate tanks presenting a high extent of thermal stratification. However, these models do not consider the effect of the thermocline transport in the calculation of the temperature distribution. Due to the inherent numerical diffusion of the multi-node modelling approach, high spatial resolution models may lead to larger simulation times compared to models with lower spatial resolutions without significantly enhancing the accuracy of their results.

This paper presented a novel 1-D multi-node model based on a hybrid continuous–discrete states modelling approach to simulate the temperatures within a TES tank with a high extent of thermal stratification. The model includes calculations for the position of a thin thermocline through the tank and its effect on temperatures due to the water transport time delay. In addition, the modelling approach is adaptable for water tanks with different extents of thermal stratification during charging and discharging.

A hybrid multi-node tank model with a spatial resolution of 12 nodes was developed for a practical hot water TES tank system presenting a poor thermal stratification during charging and a high extent of thermal stratification during discharging processes. The model was simulated and experimentally validated for a complete charging and discharging cycle using real measurements from a practical commercial tank.

The hybrid 12-node tank model was compared through simulations against the standard multi-node tank model with spatial resolutions of 12 and 60 nodes. Simulation results demonstrated that the hybrid 12-node model achieved a better agreement with the temperatures and SoC exhibited by the real tank during discharging compared to the standard models. The computational cost of the models was also compared through their simulation time ratios, with the hybrid 12-node tank model exhibiting a lower simulation time ratio than the standard 60-node tank model.

A direct comparison of the simulation errors (specifically the RMSE and MAE) of the three tank models with the experimental data also showed that the standard 60-node tank model produces the largest simulation errors in temperatures and SoC during discharging. This demonstrates that a higher spatial resolution does not necessarily guarantee accuracy in simulation results.

The presented modelling approach for hot water tanks exhibited improvements to the standard approach in three aspects: (i) the adaptability of the hybrid model to represent high and low thermal stratification during charging and discharging and the possibility to switch between these stratification conditions, (ii) the accuracy of the hybrid model to estimate the temperature distribution and the SoC of the tank, and (iii) the reduced computational cost of the hybrid model compared to standard tank models with a higher spatial resolution.

Table 6
RMSE of the hybrid 12-node model for T_2 to T_9 obtained with different Δt.

Test	Δt [s]	Layer temperature [°C]							
		T_2	T_3	T_4	T_5	T_6	T_7	T_8	T_9
Charging and discharging	1	1.68	1.39	1.48	1.69	1.74	1.97	2.28	2.45
	5	1.68	1.42	1.53	1.82	1.89	2.12	2.51	2.79
	10	1.68	2.00	2.51	3.15	3.45	3.87	4.24	4.55
Charging	1	1.72	1.67	1.51	1.61	1.41	1.42	1.42	0.73
	5	1.72	1.68	1.51	1.61	1.41	1.42	1.42	0.73
	10	1.72	1.68	1.51	1.61	1.41	1.42	1.42	0.73
Discharging	1	1.65	0.88	1.44	1.82	2.14	2.56	3.14	3.73
	5	1.65	0.97	1.58	2.10	2.43	2.86	3.55	4.26
	10	1.65	2.40	3.48	4.53	5.12	5.81	6.39	7.04

Table 7
MAE of the hybrid 12-node model for T_2 to T_9 obtained with different Δt.

Test	Δt [s]	Layer temperature [°C]							
		T_2	T_3	T_4	T_5	T_6	T_7	T_8	T_9
Charging and discharging	1	1.03	0.96	1.05	1.16	1.15	1.26	1.39	1.21
	5	1.03	0.96	1.07	1.21	1.20	1.32	1.48	1.35
	10	1.03	1.12	1.33	1.65	1.79	2.04	2.25	2.17
Charging	1	1.36	1.30	1.17	1.26	1.05	1.09	1.07	0.57
	5	1.36	1.30	1.18	1.26	1.05	1.10	1.07	0.57
	10	1.36	1.30	1.18	1.26	1.05	1.10	1.07	0.57
Discharging	1	0.6	0.48	0.89	1.05	1.32	1.53	1.88	2.14
	5	0.6	0.49	0.93	1.15	1.44	1.66	2.10	2.49
	10	0.6	0.87	1.58	2.24	2.88	3.43	3.97	4.49

Table 8
RMSE and MAE of the hybrid 12-node model for SoC and SoC_m obtained with different Δt.

Test	Δt [s]	RMSE		RMSE	
		SoC [%]	SoC_m [%]	SoC [%]	SoC_m [%]
Charging and discharging	1	3.52	1.41	3.25	1.22
	5	4.24	1.48	3.91	1.29
	10	5.12	2.56	4.63	1.94
Charging	1	4.61	1.59	4.33	1.35
	5	4.62	1.6	4.33	1.35
	10	4.62	1.6	4.33	1.35
Discharging	1	3.31	1.12	3.06	1.07
	5	3.54	1.33	3.25	1.24
	10	5.7	3.51	5	2.81

CRediT authorship contribution statement

Iván De la Cruz-Loredo: Conceptualization, Formal analysis, Investigation, Methodology, Software, Validation, Visualization, Writing – original draft. **Daniel Zinsmeister:** Conceptualization, Investigation, Data curation, Visualization, Writing – review & editing. **Thomas Licklederer:** Conceptualization, Investigation, Data curation, Visualization, Writing – review & editing. **Carlos E. Ugalde-Loo:** Conceptualization, Funding acquisition, Project administration, Resources, Supervision, Visualization, Writing – review & editing. **Daniel A. Morales:** Conceptualization, Writing – review & editing. **Héctor Bastida:** Conceptualization, Writing – review & editing. **Vedran S. Perić:** Conceptualization, Funding acquisition, Project administration, Resources, Supervision, Writing – review & editing. **Arslan Saleem:** Writing – review & editing.

Declaration of competing interest

The authors declare that they have no known competing financial interests or personal relationships that could have appeared to influence the work reported in this paper.

Data availability

Data will be made available on request.

Acknowledgments

The work presented was partly funded by the Mexican government through the National Council of Science and Technology (CONACyT). The work was also supported by FLEXIS—a project part-funded by the European Regional Development Fund (ERDF) through the Welsh Government (WEFO case number 80 836) and by the Engineering and Physical Sciences Research Council (EPSRC), UK Research and Innovation, through the projects 'Flexibility from Cooling and Storage (Flex-Cool-Store)' under grant EP/V042505/1, and 'Multi-energy Control of Cyber-Physical Urban Energy Systems (MC2)' under grant EP/T021969/1. The work of Thomas Licklederer and Daniel Zinsmeister was supported by the Federal Ministry for Economic Affairs and Energy, Germany (FKZ: 03EN3032). The work of Vedran S. Perić was supported by Deutsche Forschungsgemeinschaft (DFG), Germany (FKZ: 450821044). The construction of the CoSES laboratory was supported by Deutsche Forschungsgemeinschaft (DFG), Germany (FKZ: 350746631).

Appendix A. Commercial software engines for 1-D modelling and simulation of hot water TES tanks

1-D models of TES tanks are commonly adopted by popular commercial dynamic process simulators such as Modelica, Apros, IDA-ICE and TRNSYS to simulate energy networks at local and district scales [26,31]. These are briefly discussed next.

A.1. SimulationX

SimulationX is based on the modelling language Modelica. The integrated Green City library provides a wide range of component models of energy supply systems, including detailed models of thermal elements [53].

The library includes a stratified TES tank model, where the spatial resolution can be defined by the user. The height of the pipe connectors for charging and discharging can be defined as well. The connection can be direct or through internal heat exchangers. Fundamental heat transfer effects between neighbouring nodes include forced and natural convection, conduction, and heat losses to the environment [38].

A.2. Apros

Apros is a comprehensive software used for modelling and dynamic simulation of industrial processes. Its numerical solvers include different levels of accuracy for the solution of temperatures in solid structures and the hydraulic node pressures, flows and enthalpies [53].

Apros comprises a wide range of elements suitable for the simulation of heating and cooling systems from industrial applications. However, it is also possible to build simulation components using Simantics Constraint Language programming. The mathematical representation of TES tanks available in Apros is based on the laws of mass, momentum and energy conservation. The user can specify the spatial resolution and the dimensions of each individual calculation volume in the TES tank [54,55].

A.3. TRNSYS

TRNSYS (an acronym for TRaNsient SYStems) was originally developed for the transient simulation of solar thermal processes, but it is widely adopted to simulate solar systems, low energy buildings and HVAC systems, renewable energy systems, cogeneration, and fuel cells [39].

Several TES tanks with different geometries are included in the standard library. The components TYPE 4, 60, 340 and 534 are vertical hot water tanks. The user determines the degree of thermal stratification by defining the number of nodes. Energy balance is performed to calculate the temperature of each node. The models consider convection and the conductivity of the fluid inside the tank [39].

A.4. IDA ICE

IDA Indoor Climate and Energy (IDA ICE) is a simulation tool to accurately model buildings, its systems, and controllers. The software conducts energy balance considering climatic variations and a dynamically varying time step and enables calculation of CO_2 emissions [56]. IDA ICE's library includes thermal models for buildings, models for inter-zone airflows of buildings, and airflows through leaks and openings.

The software also includes in its library non-stratified and stratified hot water tanks. Parameters of the tanks are user-defined. For instance, heat transfer between nodes and heat exchange due to stratification are factors that may be considered in the modelling [57].

Appendix B. Mathematical description of standard 1-D multi-node tank model

The multi-node model divides the tank into an N number of equally sized fully mixed volumes or nodes, as shown in Fig. B.1. The rate of change of the sensible heat for a specific node i of the tank is given by (2) in Section 3 as a summation of heat flows.

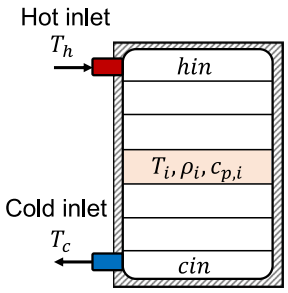

Fig. B.1. Standard 1-D multi-node model of a hot water-based TES tank.

The heat flow generated by the forced convection heat transfer $\dot{Q}_{FC,i}$ [W] is given by

$$\dot{Q}_{FC,i} = \begin{cases} c_{p,i}\rho_i \dot{V}_{in}(T_{i+1} - T_i) & \forall\, \dot{V}_{in} > 0 \\ c_{p,i}\rho_i \dot{V}_{in}(T_i - T_{i-1}) & \forall\, \dot{V}_{in} < 0 \end{cases} \tag{B.1}$$

where $\dot{V}_{in}$ [m^3/s] is the volumetric water flow in the tank, $c_{p,i}$ [J/(kg °C)] is the specific heat capacity of the water in node i at temperature T_i and ρ_i [kg/m^3] its density, and T_i [°C], T_{i+1} [°C] and T_{i-1} [°C] are the temperatures of node i and the nodes immediately above and below it. $\dot{V}_{in} > 0$ when charging the tank and $\dot{V}_{in} < 0$ when discharging the tank. Eq. (B.1) is true for nodes located in between the hot and cold tank inlets (e.g. $i = 2, 3, \ldots, N-1$ for the tank in Fig. B.1). For the nodes where tank inlets are located (i.e. nodes 1 and N in Fig. B.1), (B.1) is expressed as

$$\dot{Q}_{FC,cin} = \begin{cases} c_{p,cin}\rho_{cin} \dot{V}_{in}(T_{cin+1} - T_{cin}) & \forall\, \dot{V}_{in} > 0 \\ c_{p,cin}\rho_{cin} \dot{V}_{in}(T_{cin} - T_c) & \forall\, \dot{V}_{in} < 0 \end{cases} \tag{B.2}$$

$$\dot{Q}_{FC,hin} = \begin{cases} c_{p,hin}\rho_{hin} \dot{V}_{in}(T_h - T_{hin}) & \forall\, \dot{V}_{in} > 0 \\ c_{p,hin}\rho_{hin} \dot{V}_{in}(T_{hin} - T_{hin-1}) & \forall\, \dot{V}_{in} < 0 \end{cases} \tag{B.3}$$

where subindices '*hin*' and '*cin*' stand for hot and cold inlet nodes and T_h [°C] and T_c [°C] are the charging and discharging temperatures in the hot and cold inlets of the tank.

The heat flow generated by the natural convection heat transfer $\dot{Q}_{NC,i}$ [W] occurs from lower to upper nodes whenever a lower node presents a higher temperature than an upper node. This effect is modelled by a temperature-dependent piecewise function as

$$\dot{Q}_{NC,i} = \begin{cases} 0 & \forall\, T_{i-1} < T_i < T_{i+1} \\ \dot{Q}_{NC,i-1\to i} & \forall\, T_{i-1} > T_i < T_{i+1} \\ -\dot{Q}_{NC,i\to i+1} & \forall\, T_{i-1} < T_i > T_{i+1} \\ \dot{Q}_{NC,i-1\to i} - \dot{Q}_{NC,i\to i+1} & \forall\, T_{i-1} > T_i > T_{i+1} \end{cases} \tag{B.4}$$

where $\dot{Q}_{NC,i-1\to i}$ [W] is the natural convection heat transfer from node $i-1$ to node i, and $\dot{Q}_{NC,i\to i+1}$ [W] is the natural convection heat transfer from node i to node $i+1$. In turn, these terms are given as [38]

$$\dot{Q}_{NC,i\to i+1} = c_{p,i} g A_c (T_{i+1} - T_i) \int (\rho_{i+1} - \rho_i) dt \tag{B.5}$$

$$\dot{Q}_{NC,i-1\to i} = c_{p,i} g A_c (T_{i-1} - T_i) \int (\rho_{i-1} - \rho_i) dt \tag{B.6}$$

where A_c [m^2] is the cross-sectional area of the tank, and $\int(\rho_{i+1} - \rho_i)dt$ and $\int(\rho_{i-1} - \rho_i)dt$ [(kg s)/m^3] are the integrals of the difference in densities between nodes.

The heat flow generated by the conduction heat transfer $\dot{Q}_{K,i}$ [W] may occur through several media including the storage material and the tank's wall. For instance, thermal conductors such as internal heat exchangers and electric heaters may cause a variation in the conduc-

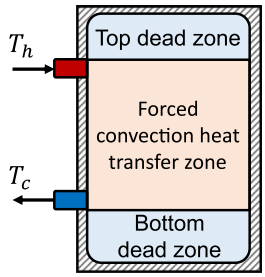

Fig. B.2. Dead zones in a TES tank.

tion heat transfer conditions from node to node. For node i, $\dot{Q}_{K,i}$ is given as

$$\dot{Q}_{K,i} = \dot{Q}_{K,i\leftrightarrow i+1} + \dot{Q}_{K,i\leftrightarrow i-1} \tag{B.7}$$

where $\dot{Q}_{K,i\leftrightarrow i+1}$ [W] is the conduction heat transfer between node i and node $i+1$, and $\dot{Q}_{K,i\leftrightarrow i-1}$ [W] is the conduction heat transfer between node i and node $i-1$. In turn, these are modelled as

$$\dot{Q}_{K,i\leftrightarrow i+1} = (k_f + k_{m,i\leftrightarrow i+1})\Delta x_i(T_{i+1} - T_i) \tag{B.8}$$

$$\dot{Q}_{K,i\leftrightarrow i-1} = (k_f + k_{m,i\leftrightarrow i-1})\Delta x_i(T_{i-1} - T_i) \tag{B.9}$$

where k_f [W/(m°C)] is the thermal conductivity coefficient of the storage medium, Δx_i [m] is the node's height ($\Delta x_i = V_i/A_c$), and $k_{m,i\leftrightarrow i+1}$ and $k_{m,i\leftrightarrow i-1}$ [W/(m°C)] are adjusting thermal conductivity coefficients representing the conduction heat transfer between nodes produced by any other media.

The heat loss $\dot{Q}_{L,i}$ is commonly modelled as a convective heat transfer between the node and the ambient through the tank's wall as [9,26]

$$\dot{Q}_{L,i} = U_i A_{w,i}(T_i - T_a) \tag{B.10}$$

where T_a [°C] is the ambient temperature, $A_{w,i}$ [m^2] is the tank's wall surface connecting the node's storage volume and the ambient, and U_i [W/(m^2 °C)] is the convective heat transfer coefficient between them. The value of U_i depends on the flow regime [43]. However, the heat loss of a storage tank in standby condition (i.e. $\dot{V}_{in} = 0$) can be experimentally characterised, as shown in [25]. Thus, U_i is given as

$$U_i = \begin{cases} U_{FC,i} & \forall\, \dot{V}_{in} \neq 0 \\ U_{0,i} & \forall\, \dot{V}_{in} = 0 \end{cases} \tag{B.11}$$

where $U_{FC,i}$ [W/(m^2 °C)] is the heat transfer coefficient due to forced convection, obtained as in [45], and $U_{0,i}$ [W/(m^2 °C)] is the heat transfer coefficient for the tank's standby condition.

The heat flow produced by internal or external heat generation sources $\dot{Q}_{G,i}$ [W] can be considered as direct heat power input to the node depending on the type of heat source.

B.1. Dead zones

The generation of dead zones or stagnation zones in TES tanks occurs when the hot and cold inlets do not produce forced convection heat transfer at the top and bottom of the tank [9]. This is shown in Fig. B.2. Unlike tank model in Fig. B.1, nodes '*hin*' and '*cin*' are not the top and bottom nodes in the tank. The modelling of the nodes within these dead zones (i.e. nodes above node '*hin*' and below node '*cin*') is given by (2) when considering $\dot{Q}_{FC,i} = 0$, that is,

$$\dot{H}_i = \dot{Q}_{NC,i} + \dot{Q}_{K,i} + \dot{Q}_{L,i} + \dot{Q}_{G,i} \tag{B.12}$$

Appendix C. Standby heat losses of the TES tank

To characterise the standby heat loss of the BSP-800 TES unit, the tank was charged to a temperature of 85 °C and left to cool down. The temperature of the tank was then recorded every 5 min over a period of 380 h at an ambient temperature around 20 °C. Then, using a spatial resolution of 1 node per layer (i.e. a 12-node tank model), the heat transfer coefficient between the storage and the environment U_0 [W/(m^2 °C)] was heuristically adjusted for each layer of the tank to fit the temperature measurements during the experiment.

Figs. C.1 and C.2 show the comparison between the temperature measurements and the SoC obtained from the experiment and simulation of the standard 12-node tank model. The SoC RMSE and MAE values of the model are 4.89% and 3.66%, respectively. Table C.1 shows the values of U_0 adopted for each layer of the tank model. These values were adopted for the standard 12-node model, the standard 60-node model, and the hybrid 12-node model.

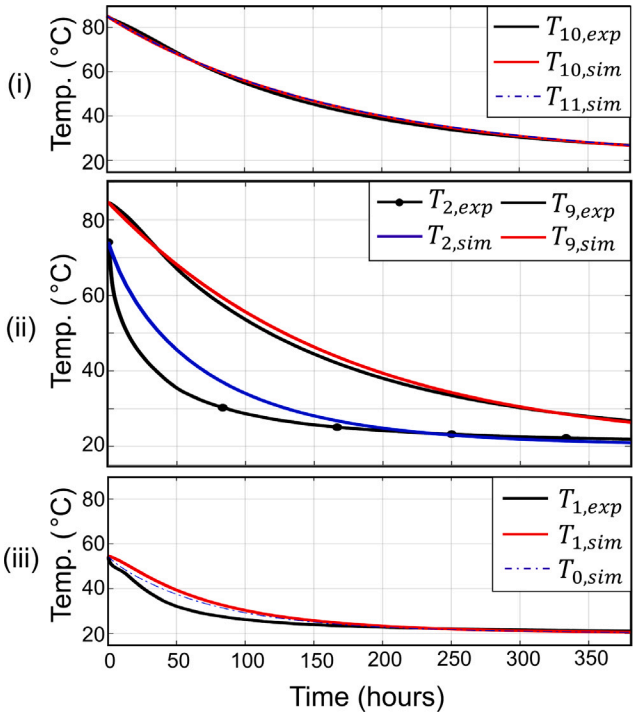

Fig. C.1. Comparison of temperature measurements between the experiment and the standard 12-node model simulation of the TES tank in standby condition for: (i) layers 11 and 10, (ii) layers 9 and 2, and (iii) layers 1 and 0.

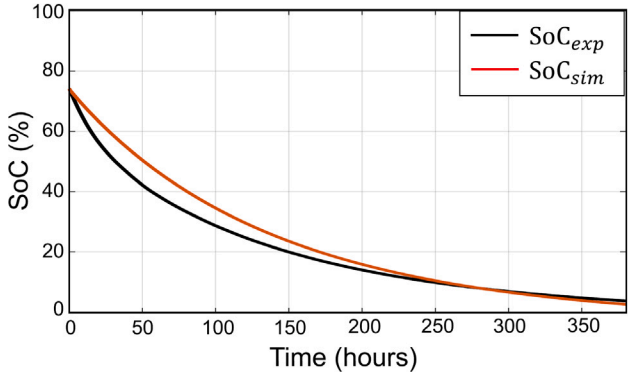

Fig. C.2. Comparison of the SoC between the experiment and the standard 12-node model simulation of the TES tank in standby condition.

Table C.1
U_0 values characterised for each layer of the standard 12-node tank model.

	U_0 [W/(m^2 °C)]											
12-node model	L_{11} 40	L_{10} 40	L_9 40	L_8 40	L_7 110	L_6 110	L_5 110	L_4 120	L_3 120	L_2 120	L_1 150	L_0 150

References

[1] Vandermeulen A, van der Heijde B, Helsen L. Controlling district heating and cooling networks to unlock flexibility: A review. Energy 2018;151:103–15. http://dx.doi.org/10.1016/j.energy.2018.03.034.

[2] De la Cruz I, Ugalde-Loo CE. District heating and cooling systems. In: Jenkins N, editor. Microgrids and local energy systems. IntechOpen; 2021, http://dx.doi.org/10.5772/intechopen.99740.

[3] Guelpa E, Verda V. Thermal energy storage in district heating and cooling systems: A review. Appl Energy 2019;252:113474. http://dx.doi.org/10.1016/j.apenergy.2019.113474.

[4] Powell KM, Edgar TF. An adaptive-grid model for dynamic simulation of thermocline thermal energy storage systems. Energy Convers Manage 2013;76:865–73. http://dx.doi.org/10.1016/j.enconman.2013.08.043.

[5] Zurigat YH, Maloney KJ, Ghajar AJ. A comparison study of one-dimensional models for stratified thermal storage tanks. J Sol Energy Eng 1989;111(3):204–10. http://dx.doi.org/10.1115/1.3268308.

[6] Cadau N, De Lorenzi A, Gambarotta A, Morini M, Rossi M. Development and analysis of a multi-node dynamic model for the simulation of stratified thermal energy storage. Energies 2019;12(22):4275. http://dx.doi.org/10.3390/en12224275.

[7] Li S-h, Zhang Y-x, Li Y, Zhang X-s. Experimental study of inlet structure on the discharging performance of a solar water storage tank. Energy Build 2014;70:490–6. http://dx.doi.org/10.1016/j.enbuild.2013.11.086.

[8] Haller MY, Yazdanshenas E, Andersen E, Bales C, Streicher W, Furbo S. A method to determine stratification efficiency of thermal energy storage processes independently from storage heat losses. Sol Energy 2010;84(6):997–1007. http://dx.doi.org/10.1016/j.solener.2010.03.009.

[9] Chandra YP, Matuska T. Stratification analysis of domestic hot water storage tanks: A comprehensive review. Energy Build 2019;187:110–31. http://dx.doi.org/10.1016/j.enbuild.2019.01.052.

[10] Haller MY, Cruickshank CA, Streicher W, Harrison SJ, Andersen E, Furbo S. Methods to determine stratification efficiency of thermal energy storage processes – Review and theoretical comparison. Sol Energy 2009;83(10):1847–60. http://dx.doi.org/10.1016/j.solener.2009.06.019.

[11] Han Y, Wang R, Dai Y. Thermal stratification within the water tank. Renew Sustain Energy Rev 2009;13(5):1014–26. http://dx.doi.org/10.1016/j.rser.2008.03.001.

[12] Coker AK. Industrial and laboratory reactors – Chemical reaction hazards and process integration of reactors. In: Ludwig's applied process design for chemical and petrochemical plants. Elsevier; 2015, p. 1095–208. http://dx.doi.org/10.1016/B978-0-08-094242-1.00021-8.

[13] Lavan Z, Thompson J. Experimental study of thermally stratified hot water storage tanks. Sol Energy 1977;19(5):519–24. http://dx.doi.org/10.1016/0038-092X(77)90108-6.

[14] Hahne E, Chen Y. Numerical study of flow and heat transfer characteristics in hot water stores. Sol Energy 1998;64(1):9–18. http://dx.doi.org/10.1016/S0038-092X(98)00051-6.

[15] Cole R, Bellinger F. Natural thermal stratification in tanks. Phase 1 final report, 1982, http://dx.doi.org/10.2172/5246085.

[16] Weiss J, Ortega-Fernández I, Müller R, Bielsa D, Fluri T. Improved thermocline initialization through optimized inlet design for single-tank thermal energy storage systems. J Energy Storage 2021;42:103088. http://dx.doi.org/10.1016/j.est.2021.103088.

[17] Cho H-I, Cabrera D, Patel MK. Estimation of energy savings potential through hydraulic balancing of heating systems in buildings. J Build Eng 2020;28:101030. http://dx.doi.org/10.1016/j.jobe.2019.101030.

[18] Yu ZJ, Huang G, Haghighat F, Li H, Zhang G. Control strategies for integration of thermal energy storage into buildings: State-of-the-art review. Energy Build 2015;106:203–15. http://dx.doi.org/10.1016/j.enbuild.2015.05.038.

[19] Yang X, Svendsen S. Improving the district heating operation by innovative layout and control strategy of the hot water storage tank. Energy Build 2020;224:110273. http://dx.doi.org/10.1016/j.enbuild.2020.110273.

[20] Castell A, Medrano M, Solé C, Cabeza L. Dimensionless numbers used to characterize stratification in water tanks for discharging at low flow rates. Renew Energy 2010;35(10):2192–9. http://dx.doi.org/10.1016/j.renene.2010.03.020.

[21] Rendall J, Abu-Heiba A, Gluesenkamp K, Nawaz K, Worek W, Elatar A. Nondimensional convection numbers modeling thermally stratified storage tanks: Richardson's number and hot-water tanks. Renew Sustain Energy Rev 2021;150:111471. http://dx.doi.org/10.1016/j.rser.2021.111471.

[22] Bahnfleth W, Song J, Cimbala J. Measured and modeled charging of a stratified chilled water thermal storage tank with slotted pipe diffusers. HVAC R Res 2003;9(4):467–91. http://dx.doi.org/10.1080/10789669.2003.10391081.

[23] Nelson JEB, Balakrishnan AR, Murthy SS. Transient analysis of energy storage in a thermally stratified water tank. Int J Energy Res 1998;22(10):867–83. http://dx.doi.org/10.1002/(SICI)1099-114X(199808)22:10<867::AID-ER410>3.0.CO;2-L.

[24] Wang Z, Zhang H, Dou B, Huang H, Wu W, Wang Z. Experimental and numerical research of thermal stratification with a novel inlet in a dynamic hot water storage tank. Renew Energy 2017;111:353–71. http://dx.doi.org/10.1016/j.renene.2017.04.007.

[25] Fan J, Furbo S. Thermal stratification in a hot water tank established by heat loss from the tank. Sol Energy 2012;86(11):3460–9. http://dx.doi.org/10.1016/j.solener.2012.07.026.

[26] Campos Celador A, Odriozola M, Sala J. Implications of the modelling of stratified hot water storage tanks in the simulation of CHP plants. Energy Convers Manage 2011;52(8):3018–26. http://dx.doi.org/10.1016/j.enconman.2011.04.015.

[27] Bastida H, Ugalde-Loo CE, Abeysekera M, Qadrdan M, Wu J, Jenkins N. Dynamic modelling and control of thermal energy storage. Energy Procedia 2019;158:2890–5. http://dx.doi.org/10.1016/j.egypro.2019.01.942.

[28] Huang T, Yang X, Svendsen S. Multi-mode control method for the existing domestic hot water storage tanks with district heating supply. Energy 2020;191:116517. http://dx.doi.org/10.1016/j.energy.2019.116517.

[29] Morales Sandoval DA, De La Cruz Loredo I, Bastida H, Badman JJR, Ugalde-Loo CE. Design and verification of an effective state-of-charge estimator for thermal energy storage. IET Smart Grid 2021;4(2):202–14. http://dx.doi.org/10.1049/stg2.12024.

[30] Ferrari M, Cuneo A, Pascenti M, Traverso A. Real-time state of charge estimation in thermal storage vessels applied to a smart polygeneration grid. Appl Energy 2017;206:90–100. http://dx.doi.org/10.1016/j.apenergy.2017.08.062.

[31] del Hoyo Arce I, Herrero López S, López Perez S, Rämä M, Klobut K, Febres JA. Models for fast modelling of district heating and cooling networks. Renew Sustain Energy Rev 2018;82:1863–73. http://dx.doi.org/10.1016/j.rser.2017.06.109.

[32] Zinsmeister D, Lickleder T, Christange F, Tzscheutschler P, Perić VS. A comparison of prosumer system configurations in district heating networks. Energy Rep 2021;7:430–9. http://dx.doi.org/10.1016/j.egyr.2021.08.085.

[33] Dinçer Í, Rosen MA. Thermal energy storage: systems and applications. 1st ed.. Wiley; 2010, http://dx.doi.org/10.1002/9780470970751, URL https://onlinelibrary.wiley.com/doi/book/10.1002/9780470970751.

[34] Newton BJ. Modeling of solar storage tanks. University of Wisconsin-Madison; 1995, URL https://minds.wisconsin.edu/handle/1793/7803.

[35] Baeten B, Confrey T, Pecceu S, Rogiers F, Helsen L. A validated model for mixing and buoyancy in stratified hot water storage tanks for use in building energy simulations. Appl Energy 2016;172:217–29. http://dx.doi.org/10.1016/j.apenergy.2016.03.118.

[36] Bulnes FK, Rendall J, Gluesenkamp KR. Comparison of plug flow and multi-node stratified tank modeling approaches regarding computational efficiency and accuracy. 2020, URL https://www.osti.gov/biblio/1756251.

[37] Younes A, Fahs M, Ackerer P. A new approach to avoid excessive numerical diffusion in Eulerian-Lagrangian methods. Commun Numer Methods Eng 2007;24(11):897–910. http://dx.doi.org/10.1002/cnm.996.

[38] SimulationX Help Center, URL http://doc.simulationx.com/4.0/1033/Default.htm#Libraries/GreenCity/GreenBuilding/HeatStorage/HeatStorageStratified.htm.

[39] TRNSYS - Official Website, URL https://sel.me.wisc.edu/trnsys/trnlib/library16.htm.

[40] Li P-W, Chan CL. Thermal storage system configurations and basic operation. In: Thermal energy storage analyses and designs. Elsevier; 2017, p. 7–19. http://dx.doi.org/10.1016/B978-0-12-805344-7.00002-X.

[41] What is an S-function? - MATLAB & Simulink, URL https://www.mathworks.com/help/simulink/sfg/what-is-an-s-function.html.

[42] Perić VS, Hamacher T, Mohapatra A, Christiange F, Zinsmeister D, Tzscheutschler P, Wagner U, Aigner C, Witzmann R. CoSES laboratory for combined energy systems at TU munich. In: 2020 IEEE power & energy society general meeting (PESGM). IEEE; 2020, p. 1–5. http://dx.doi.org/10.1109/PESGM41954.2020.9281442.

[43] Stratification cylinders | WOLF Heating, air conditioning, ventilation, URL https://www.wolf.eu/en-de/products/stratification-cylinders.

[44] Gas condensing boilers CGB-2 series | WOLF Heating, Air Conditioning, Ventilation, URL https://www.wolf.eu/en-de/products/gas-condensing-boilers-cgb-2.

[45] Bastida H, Ugalde-Loo CE, Abeysekera M, Qadrdan M. Dynamic modeling and control of a plate heat exchanger. In: 2017 IEEE conference on energy internet and energy system integration (EI2). IEEE; 2017, p. 1–6. http://dx.doi.org/10.1109/EI2.2017.8245736.

[46] Benakopoulos T, Salenbien R, Vanhoudt D, Svendsen S. Improved control of radiator heating systems with thermostatic radiator valves without pre-setting function. Energies 2019;12(17):3215. http://dx.doi.org/10.3390/en12173215.
[47] Jin X, Zhang X, Luo Y. A calculation method for the floor surface temperature in radiant floor system. Energy Build 2010;42(10):1753–8. http://dx.doi.org/10.1016/j.enbuild.2010.05.011.
[48] Missaoui S, Driss Z, Slama RB, Chaouachi B. Effects of pipe turns on vertical helically coiled tube heat exchangers for water heating in a household refrigerator. Int J Air-Cond Refrig 2022;30(1):6. http://dx.doi.org/10.1007/s44189-022-00005-5.
[49] Kewin Titus A, Khaja Fareedudeen Ahmed KS, Sabarish Kumar P, Santhosh D, Arun Vasantha Geethan K. Design and analysis of helical coil heat exchanger. IOP Conf Ser: Mater Sci Eng 2020;923(1):012016. http://dx.doi.org/10.1088/1757-899X/923/1/012016.
[50] Munson BR, Rothmayer AP, Okiishi TH, Huebsch WW. Fundamentals of fluid mechanics. 7th ed.. Hoboken, NJ: Wiley; 2012.
[51] Dahash A, Ochs F, Janetti MB, Streicher W. Advances in seasonal thermal energy storage for solar district heating applications: A critical review on large-scale hot-water tank and pit thermal energy storage systems. Appl Energy 2019;239:296–315. http://dx.doi.org/10.1016/j.apenergy.2019.01.189.
[52] Toyoshima M, Okawa S. An effect of a horizontal buoyant jet on the temperature distribution inside a hot water storage tank. Int J Heat Fluid Flow 2013;44:403–13. http://dx.doi.org/10.1016/j.ijheatfluidflow.2013.07.009.
[53] Unger R, Schwan T, Mikoleit B, Bäker B, Kehrer C, Rodemann T. "Green Building" - Modelling renewable building energy systems and electric mobility concepts using modelica. 2012, p. 897–906. http://dx.doi.org/10.3384/ecp12076897.
[54] Technical data manual, Apros® Product specifications.
[55] Apros® Dynamic process simulation software | VTT, URL https://www.vttresearch.com/en/ourservices/aprosr-dynamic-process-simulation-software.
[56] IDA ICE - Simulation Software | EQUA, URL https://www.equa.se/en/ida-ice.
[57] AB, EQUA simulation, IDA Indoor Climate and Energy. User manual. 2013, Version 4.5.